MULTISCALE MODEL. SIMUL.
Vol. 18, No. 4, pp. 1409–1434

A MULTISCALE REDUCED BASIS METHOD FOR THE SCHRÖDINGER EQUATION WITH MULTISCALE AND RANDOM POTENTIALS*

JINGRUN CHEN†, DINGJIONG MA‡, AND ZHIWEN ZHANG§

Abstract. The semiclassical Schrödinger equation with multiscale and random potentials often appears when studying electron dynamics in heterogeneous quantum systems. As time evolves, the wave function develops high-frequency oscillations in both the physical space and the random space, which poses severe challenges for numerical methods. To address this problem, in this paper we propose a multiscale reduced basis method, where we construct multiscale reduced basis functions using an optimization method and the proper orthogonal decomposition method in the physical space and employ the quasi-Monte Carlo method in the random space. Our method is verified to be efficient: the spatial grid size is only proportional to the semiclassical parameter and (under suitable conditions) an almost first-order convergence rate is achieved in the random space with respect to the sample number. Several theoretical aspects of the proposed method, including how to determine the number of samples in the construction of multiscale reduced basis and convergence analysis, are studied with numerical justification. In addition, we investigate the Anderson localization phenomena for the Schrödinger equation with correlated random potentials in both 1-dimensional and 2-dimensional space.

Key words. random Schrödinger equation, multiscale reduced basis function, optimization method, quasi-Monte Carlo method, Anderson localization

AMS subject classifications. 35J10, 35Q41, 65M60, 65K10, 74Q10

DOI. 10.1137/19M127389X

1. Introduction.

The semiclassical Schrödinger equation describes electron dynamics in the semiclassical regime. Applications of such an equation can be found in Bose–Einstein condensation, graphene, semiconductors, topological insulators, etc. When propagating in a (quasi-)periodic microstructure, electrons experience a multiscale potential. As a consequence, the electron wave function develops high-frequency oscillations, which poses severe challenges from the numerical perspective. Brute-force methods are very costly and asymptotics-based methods have been proposed in the literature; see [28] for a review and references therein.

In [2], Anderson proposed to study localized eigenstates in a tight-binding model with random potentials. This model was soon to be generalized to the random Schrödinger equation, i.e., the Schrödinger equation with a random potential. In this case, electrons are found to be localized provided that the strength of randomness is sufficiently large. The randomness can be realized in an experiment by enhancing the

*Received by the editors July 10, 2019; accepted for publication (in revised form) July 30, 2020; published electronically October 8, 2020.
https://doi.org/10.1137/19M127389X
Funding: The first author was supported by National Natural Science Foundation of China via grants 11971021 and 21602149, and National Key R&D Program of China (2018YFB0204404). The second author was supported by Hong Kong RGC grants (Projects 27300616, 17300817, and 17300318) and National Natural Science Foundation of China via grant 11601457, Seed Funding Programme for Basic Research (HKU), and Basic Research Programme (JCYJ20180307151603959) of The Science, Technology and Innovation Commission of Shenzhen Municipality.
†School of Mathematical Sciences, Soochow University, Suzhou, Jiangsu, 215006 (jingrunchen@suda.edu.cn).
‡Department of Mathematics, The University of Hong Kong, Hong Kong (martin35@hku.hk).
§Corresponding author. Department of Mathematics, The University of Hong Kong, Hong Kong, 999077 (zhangzw@hku.hk).

disorder of impurities in a material. Due to the importance of this model, Anderson was awarded the Nobel Prize in physics in 1977. In the presence of multiscale and random potentials, the electron wave function develops high-frequency oscillations in both the physical space and the random space, making numerical approximations even more difficult.

In this paper, we study the following Schrödinger equation with random potential in the semiclassical regime:

$$
\begin{cases} i\varepsilon\partial_t\psi^\varepsilon = -\dfrac{\varepsilon^2}{2}\Delta\psi^\varepsilon + v^\varepsilon(\mathbf{x},\omega)\psi^\varepsilon, \quad \mathbf{x}\in D, \quad \omega\in\Omega, \quad t\in\mathbb{R}, \\ \psi^\varepsilon \in H^1_{\mathrm{P}}(D), \quad \omega\in\Omega, \quad t\in\mathbb{R}, \\ \psi^\varepsilon|_{t=0} = \psi_{\mathrm{in}}(\mathbf{x}), \quad \mathbf{x}\in D, \end{cases} \tag{1}
$$

where $0<\varepsilon\ll 1$ is an effective Planck constant describing the microscopic and macroscopic scale ratio, d is the spatial dimension, $v^\varepsilon(\mathbf{x},\omega)$ is the given random potential, $\psi^\varepsilon=\psi^\varepsilon(t,\mathbf{x},\omega)$ is the electron wave function, and $\psi_{\mathrm{in}}(\mathbf{x})$ is the initial datum. Here $D=[0,1]^d$ is the spatial domain and $H^1_{\mathrm{P}}(D)=\{\psi|\psi\in H^1(D)$ and ψ is periodic over D$\}$.

Equation (1) can be used to model electron transport in a disordered medium in a single-electron picture where the electron interaction is ignored. It is customary to write the semiclassical Schrödinger equation and the multiscale and random potential with a single parameter ε. But there is no reason that the parameter of the multiscale and random potential should be the same as the semiclassical parameter; see section 5 for details on the parameterization of the multiscale and random potential $v^\varepsilon(\mathbf{x},\omega)$.

The existence of Anderson localization is closely related to the electron wave function in (1). To be specific, assume $\psi^\varepsilon(t,\mathbf{x},\omega)$ has zero mean with respect to the measure ρ induced by $v^\varepsilon(\mathbf{x},\omega)$ and denote by $A(t)=\mathbb{E}[\int_{R^d}|\mathbf{x}|^2|\psi^\varepsilon|^2d\mathbf{x}]_\rho$ the second-order moment of the position density. When the strength of disorder is small, an electron undergoes a diffusion process with $A(t)=2C_dt$, $C_d>0$. In the presence of a strong disorder, however, $A(t)$ converges to a time-independent quantity, i.e., $\lim_{t\to\infty}A(t)=C$, which implies the localization of the electron and the system undergoes a metal-insulator transition [37, 16]. When $d=1$, localization always occurs for (1) with random potential [2]. When $d\geq 2$, the situation becomes complicated. Some analytical results show that localization occurs when the strength of disorder is large [20, 1]. This motivates us to study Anderson localization in the presence of correlated random potentials [39].

When the potential is deterministic, i.e., $v^\varepsilon(\mathbf{x},\omega)=v^\varepsilon(\mathbf{x})$, many numerical methods have been proposed; see [5, 18, 44, 30, 17, 29, 11, 10, 8], for example. When the potential is random, not as much work has been done in the computational mathematics community; see [36, 3, 45, 27]. As mentioned above, the major difficulty is that the wave function ψ^ε develops high-frequency oscillations in both the physical space and the random space, which requires tremendous computational resources. Our goal here is to develop an efficient numerical method to solve this challenging problem.

Our work is motivated by the multiscale finite element method (FEM) for solving elliptic problems with multiscale coefficients [23, 15]. The multiscale FEM is capable of correctly capturing the large scale components of the multiscale solution on a coarse grid without accurately resolving all the small scale features in the solution. This is accomplished by incorporating the local microstructures of the differential operator into the multiscale FEM basis functions. Recently, several relevant works on constructing localized basis functions that approximate the elliptic operator with het-

erogeneous coefficients have been proposed. In [35], Målqvist and Peterseim construct localized multiscale basis functions using a modified variational multiscale method. The exponentially decaying property of these modified bases have been shown both theoretically and numerically. Meanwhile, Owhadi [40, 41] reformulates the multiscale problem from the perspective of decision theory using the idea of gamblets as the modified basis. Hou and Zhang [26] extend these works such that localized basis functions can also be constructed for higher-order strongly elliptic operators. Very recently, Hou, Ma, and Zhang proposed to build a localized multiscale stochastic basis to solve elliptic problems with multiscale and random coefficients [24].

In this paper, we propose a multiscale reduced basis method to solve the Schrödinger equation with random potentials in the semiclassical regime. Our method consists of offline and online stages. In the offline stage, we apply an optimization approach to systematically construct localized multiscale reduced basis functions on each patch associated with each coarse grid point These basis functions provide nearly optimal approximation to the random Schrödinger operator. In the online stage, we use these basis functions to approximate the physical space of the solution and the quasi-Monte Carlo (qMC) method to approximate the random space of the solution, respectively. We find the proposed method is efficient in the sense that the number of basis functions is only proportional to ε and the number of samples in qMC is inversely proportional to a power of ε. Under some conditions, we conduct the convergence analysis of the proposed method with numerical verification. Moreover, we study how to determine the number of samples in the offline stage such that the corresponding multiscale reduced basis functions provide an accurate an approximation of the solution space. Finally, we investigate the existence of Anderson localization for correlated random potentials.

The rest of the paper is organized as follows. For completeness, in section 2, we introduce multiscale basis functions for the deterministic Schrödinger equation in a semiclassical regime and discuss some properties of the basis functions. In section 3, we propose a multiscale reduced basis method to solve the random Schrödinger equation. Analysis results are presented in section 4 and numerical experiments, including both 1-dimensional (1D) and 2-dimensional (2D) examples, are conducted to demonstrate the convergence and efficiency of the proposed method in section 5. Conclusions and discussions are drawn in section 6.

2. Multiscale basis functions for deterministic Schrödinger equations.

In this section, we briefly review the construction of multiscale basis functions based on an optimization approach to solve the Schrödinger equation with a deterministic potential. Some properties of the multiscale basis functions are also given.

2.1. Construction of multiscale basis functions.

In the deterministic case, we consider the following problem:

$$\begin{cases} i\varepsilon\partial_t\psi^\varepsilon = -\dfrac{\varepsilon^2}{2}\Delta\psi^\varepsilon + v^\varepsilon(\mathbf{x})\psi^\varepsilon, \quad \mathbf{x}\in D, \quad t\in\mathbb{R}, \\ \psi^\varepsilon \in H^1_{\mathrm{P}}(D), \\ \psi^\varepsilon|_{t=0} = \psi_{\mathrm{in}}(\mathbf{x}). \end{cases} \tag{2}$$

$\psi_{\mathrm{in}}(\mathbf{x})$ is the initial data over D. Defining the Hamiltonian operator $\mathcal{H}(\cdot) \equiv -\frac{\varepsilon^2}{2}\Delta(\cdot) + v^\varepsilon(\mathbf{x})(\cdot)$ and introducing the following energy notation $||\cdot||_V$ for the Hamiltonian

operator,

$$||\psi^\varepsilon||_V = \frac{1}{2}(\mathcal{H}\psi^\varepsilon, \psi^\varepsilon) = \frac{1}{2}\int_D \frac{\varepsilon^2}{2}|\nabla\psi^\varepsilon|^2 + v^\varepsilon(\mathbf{x})|\psi^\varepsilon|^2 \mathrm{d}\mathbf{x}. \tag{3}$$

Note that (3) does not define a norm since v^ε usually can be negative, and thus the bilinear form associated with this notation is not coercive, which is quite different from the case of elliptic equations. However, this does not mean that available approaches [25, 4, 35, 41, 26, 33] cannot be used for the Schrödinger equation. In fact, we shall utilize a similar idea to construct localized multiscale basis functions on a coarse mesh by an optimization approach using the above energy notation $||\cdot||_V$ for the Hamiltonian operator.

To construct such localized multiscale basis functions, we first partition the physical domain D into a set of regular coarse elements with grid size H. For example, we divide D into a set of nonoverlapping triangles $\mathcal{T}_H = \cup\{K\}$, such that no vertex of one triangle lies in the interior of the edge of another triangle. On each element K, we define a set of nodal bases $\{\varphi_{j,K}, j = 1, \ldots, k\}$ with k being the number of nodes of the element. From now on, we neglect the subscript K for notational convenience. The functions $\varphi_i(\mathbf{x})$ are called measurement functions, which are chosen as the characteristic functions on each coarse element in [26, 41] and piecewise linear basis functions in [35]. In [33, 24], it is found that the usage of FEM nodal basis functions reduces the approximation error and thus the same setting is adopted in the current work.

Let $\mathcal{N}$ denote the set of vertices of $\mathcal{T}_H$ (removing the repeated vertices due to the periodic boundary condition) and N_H be the number of vertices. For every vertex $\mathbf{x}_i \in \mathcal{N}$, let $\varphi_i^H(\mathbf{x})$ denote the corresponding nodal basis function, i.e., $\varphi_i^H(\mathbf{x}_j) = \delta_{ij}$. Since all the nodal basis functions $\varphi_i(\mathbf{x})$ are continuous across the boundaries of the elements, we have

$$V^H = \{\varphi_i^H(\mathbf{x}) : i = 1, \ldots, N_H\} \subset H^1_{\mathrm{P}}(D).$$

Then, we can solve optimization problems to obtain the multiscale basis functions. Specifically, let $\phi_i(\mathbf{x})$ be the minimizer of the following constrained optimization problem

$$\phi_i = \operatorname*{arg\,min}_{\phi \in H^1_{\mathrm{P}}(D)} ||\phi||_V \tag{4}$$

$$\text{s.t.} \int_D \phi\varphi_j^H \mathrm{d}\mathbf{x} = \delta_{i,j} \ \forall 1 \le j \le N_H. \tag{5}$$

The superscript ε is dropped for notational simplicity and the periodic boundary condition is incorporated into the above optimization problem through the solution space $H^1_{\mathrm{P}}(D)$.

In general, one cannot solve the above optimization problem analytically. Therefore, we use numerical methods to solve it. Specifically, we partition the physical domain D into a set of nonoverlapping fine triangles with size $h \ll \varepsilon$. Then, we use standard FEM to discretize $\phi_i(\mathbf{x})$, $\varphi_j^H(\mathbf{x})$, $1 \le i, j \le N_H$. On the discrete level, the optimization problem (4)–(5) is reduced to a constrained quadratic optimization problem; see (19) in section 3.3, which can be efficiently solved using Lagrange multiplier methods. Finally, with these multiscale FEM basis functions $\{\phi_i(\mathbf{x})\}_{i=1}^{N_H}$, we can solve the Schrödinger equation (2) using the Galerkin method.

Remark 2.1. In analogy to the multiscale FEM [23, 15], the multiscale basis functions $\{\phi_i(\mathbf{x})\}_{i=1}^{N_H}$ are defined on coarse elements with grid size H. However, they are

represented by a fine-scale FEM basis with grid size h, which can be precomputed and done in parallel.

Remark 2.2. The notation $||\cdot||_V$ in (3) does not define a norm. However, as long as the potential $v^\varepsilon(\mathbf{x})$ is bounded and the fine grid size h is small enough, the discrete problem of (4)–(5) is convex and thus admits a unique solution; see [26, 33] for details.

Remark 2.3. Multiple choices are available in the literature to construct multiscale basis functions, such as the original multiscale FEM [25, 23] and the gamblet method [41]. One issue associated with the multiscale FEM is how to impose appropriate boundary conditions for local cell problems. This issue is removed in the optimization approach (4)–(5) which is globally defined. By taking advantage of the exponential decay of multiscale basis functions, we can restrict global optimization problems (4)–(5) to subdomain optimization problems (10)–(12), and reduce the computational cost significantly. The gamblet method [41] was originally proposed for second-order elliptic problems, and later the optimization method [26] was developed for elliptic problems, including high-order problems. Since the fourth-order Schrödinger equation is often used in physics [32], we therefore employ the optimization approach, as we have done in [10, 8].

2.2. Exponential decay of the multiscale finite element basis functions. It can be proved that the multiscale basis functions $\{\phi_i(\mathbf{x})\}_{i=1}^{N_H}$ decay exponentially fast away from its associated vertex $\mathbf{x}_i \in \mathcal{N}_c$ under certain conditions. This allows us to localize the basis functions to a relatively smaller domain and reduce the computational cost. We first define a series of nodal patches $\{D_\ell\}$ associated with $\mathbf{x}_i \in \mathcal{N}$ as

$$D_0 := \text{supp}\{\varphi_i\} = \cup\{K \in \mathcal{T}_H | \mathbf{x}_i \in K\}, \tag{6}$$

$$D_\ell := \cup\{K \in \mathcal{T}_H | K \cap \overline{D_{\ell-1}} \neq \emptyset\}, \quad \ell = 1, 2, \ldots. \tag{7}$$

Assumption 2.1. We assume the potential $v^\varepsilon(\mathbf{x})$ is bounded, i.e., $V_0 := ||v^\varepsilon(\mathbf{x})||_{L^\infty(D)} < +\infty$ and the grid size H of $\mathcal{T}_H$ satisfies

$$\sqrt{V_0} H/\varepsilon \lesssim 1, \tag{8}$$

where $\lesssim$ means bounded from above by a constant.

Under this resolution assumption for the coarse mesh, many typical potentials in the Schrödinger equation (2) can be treated as a perturbation to the kinetic operator. Thus, they can be computed using our method. Then, we can show that the multiscale finite element basis functions have the exponentially decaying property.

PROPOSITION 2.2 (exponentially decaying property). *Under the resolution condition of the coarse mesh, i.e.,* (8)*, there exist constants* $C > 0$ *and* $0 < \beta < 1$ *independent of* H*, such that*

$$||\nabla \phi_i(\boldsymbol{x})||_{L^2(D\setminus D_\ell)} \leq C\beta^\ell ||\nabla \phi_i(\boldsymbol{x})||_{L^2(D)} \tag{9}$$

for any $i = 1, 2, \ldots, N_H$.

Proof of (9) will be given in [9]. The main idea is to combine an iterative Caccioppoli-type argument [35, 33] and some refined estimates with respect to ε.

The exponential decay of the basis functions enables us to localize the support sets of the basis functions $\{\phi_i(\mathbf{x})\}_{i=1}^{N_H}$, so that the corresponding stiffness matrix is sparse

and the computational cost is reduced. In practice, we define a modified constrained optimization problem as follows:

$$\phi_i^{\mathrm{loc}} = \underset{\phi \in H^1_{\mathrm{P}}(D)}{\arg\min} ||\phi||_V \tag{10}$$

$$\text{s.t.} \int_{D_{l^*}} \phi \varphi_j^H \mathrm{d}\mathbf{x} = \delta_{i,j} \ \forall 1 \le j \le N_H, \tag{11}$$

$$\phi(\mathbf{x}) = 0, \ \mathbf{x} \in D \backslash D_{l^*}, \tag{12}$$

where D_{l^*} is the support set of the localized multiscale basis function $\phi_i^{\mathrm{loc}}(\mathbf{x})$ and the choice of the integer l^* depends on the decaying speed of $\phi_i^{\mathrm{loc}}(\mathbf{x})$. In (11) and (12), we have used the fact that $\phi_i(\mathbf{x})$ has the exponentially decaying property so that we can localize the support set of $\phi_i(\mathbf{x})$ to a smaller domain D_{l^*}. In numerical experiments, we find that a small integer $l^* \sim \log(L/H)$ will give accurate results, where L is the diameter of domain D. Moreover, the optimization problem (10)–(12) can be solved in parallel. Therefore, the exponentially decaying property significantly reduces our computational cost in constructing basis functions and computing the solution of the Schrödinger equation (2).

With the localized multiscale finite element basis functions $\{\phi_i^{\mathrm{loc}}(\mathbf{x})\}_{i=1}^{N_H}$, we can approximate the wave function by $\psi^\varepsilon(\mathbf{x}, t) = \sum_{i=1}^{N_H} c_i(t)\phi_i^{\mathrm{loc}}(\mathbf{x})$ using the Galerkin method.

3. Multiscale reduced basis functions for the random Schrödinger equation.

3.1. Parameterization of the random potential. The random potential $v^\varepsilon(\mathbf{x}, \omega)$ is used to model the disorder in a given material. Specifically, we assume $v^\varepsilon(\mathbf{x}, \omega)$ is a second-order random field, i.e., $v^\varepsilon(\mathbf{x}, \omega) \in L^2(D, \Omega)$, with mean $\mathbb{E}[v^\varepsilon(\mathbf{x}, \omega)] = \bar{v}^\varepsilon(\mathbf{x})$ and covariance kernel $C(\mathbf{x}, \mathbf{y})$. For example, we can choose the covariance kernel as

$$C(\mathbf{x}, \mathbf{y}) = \sigma^2 \exp\Big(- \sum_{i=1}^{d} \frac{|x_i - y_i|^2}{2l_i^2} \Big), \tag{13}$$

where σ is a constant and l_i's are the correlation lengths in each dimension. We also assume that the random potential $v^\varepsilon(\mathbf{x}, \omega)$ is almost surely bounded, namely, there exist $v_{\max}$ and $v_{\min}$, such that

$$P(\omega \in \Omega \mid v^\varepsilon(\mathbf{x}, \omega) \in [v_{\min}, v_{\max}] \ \forall \mathbf{x} \in D) = 1. \tag{14}$$

The circulant embedding method [14] and Karhunen–Loève (KL) expansion method [31, 34] are commonly used to generate samples of $v^\varepsilon(\mathbf{x}, \omega)$, and the latter will be used in the current work. The KL expansion of $v^\varepsilon(\mathbf{x}, \omega)$ reads as

$$v^\varepsilon(\mathbf{x}, \omega) = \bar{v}^\varepsilon(\mathbf{x}) + \sum_{i=1}^{\infty} \sqrt{\lambda_i} \xi_i(\omega) v_i(\mathbf{x}), \tag{15}$$

where $\xi_i(\omega)$'s are mean-zero and uncorrelated random variables, i.e., $\mathbb{E}[\xi_i] = 0$, $\mathbb{E}[\xi_i \xi_j] = \delta_{ij}$, and $\{\lambda_i, v_i(\mathbf{x})\}_{i=1}^{\infty}$ are the eigenpairs of the covariance kernel $C(\mathbf{x}, \mathbf{y})$. Generally, λ_i's are sorted in a descending order and their decay rates depend on the regularity of the covariance kernel. It has been proven that an algebraic decay

rate, i.e., $\lambda_i = \mathcal{O}(i^{-\gamma})$, is achieved asymptotically if the covariance kernel is of finite Sobolev regularity, and an exponential decay rate is achieved, i.e., $\lambda_i = \mathcal{O}(e^{-\gamma i})$ for some $\gamma > 0$ if the covariance kernel is piecewise analytic [42].

In practice, we truncate the KL expansion (15) into its first m terms and obtain a parameterization of the random potential as

$$v_m^\varepsilon(\mathbf{x}, \omega) = \bar{v}^\varepsilon(\mathbf{x}) + \sum_{i=1}^{m} \sqrt{\lambda_i}\xi_i(\omega)v_i(\mathbf{x}), \tag{16}$$

which will be used in both analysis and numerics in the remaining part of the paper.

Remark 3.1. The decay rate of λ_i also depends on the correlation lengths l_i, $i = 1, \ldots, d$, of the random field $v^\varepsilon(\mathbf{x}, \omega)$. A small correlation length results in a slow decay of the eigenvalues. When the correlation lengths approach zero, the random field $v^\varepsilon(\mathbf{x}, \omega)$ becomes a spatially white noise, which is the case used in the original physics paper [2].

3.2. Construction of the multiscale reduced basis functions. For the random Schrödinger equation (1), it is prohibitively expensive to construct multiscale basis functions for each realization of the random potential using (10)–(12). To address this issue, we use a model reduction method to build a small number of reduced basis functions that enable us to obtain multiscale basis functions in a cheaper way without loss of approximation accuracy.

For every $\mathbf{x}_k \in \mathcal{N}$, we first compute a set of samples of multiscale basis functions associated to the vertex $\mathbf{x}_k$. Specifically, let $\{v^\varepsilon(\mathbf{x}, \omega_q)\}_{q=1}^Q$ be samples of the random potential that are obtained using the Monte Carlo (MC) method or the qMC method, where Q is the number of samples. Denote by $\zeta_0^k(\mathbf{x}) = \frac{1}{Q}\sum_{q=1}^Q \phi_k^{\mathrm{loc}}(\mathbf{x}, \omega_q)$ the sample mean of the basis functions, and $\tilde{\phi}_k^{\mathrm{loc}}(\mathbf{x}, \omega_q) = \phi_k^{\mathrm{loc}}(\mathbf{x}, \omega_q) - \zeta_0^k(\mathbf{x})$ is the fluctuation of the kth basis function.

We apply the proper orthogonal decomposition (POD) method [6, 43] to $V = \{\tilde{\phi}_k^{\mathrm{loc}}(\mathbf{x}, \omega_q)\}_{q=1}^Q$ and build a set of basis functions $\{\zeta_1^k(\mathbf{x}), \zeta_2^k(\mathbf{x}), \ldots, \zeta_{m_k}^k(\mathbf{x})\}$ with $m_k \ll Q$ that optimally approximates V. Quantitatively, we have the following approximating property.

PROPOSITION 3.1. *Let $\lambda_1 \geq \lambda_2 \geq \cdots \geq \lambda_{m_k} \geq \lambda_{m_k+1} \geq \cdots > 0$ be positive eigenvalues of the covariance kernel associated with the snapshot of the fluctuations V and the corresponding eigenfunctions are $\zeta_1^k(\boldsymbol{x})$, …, $\zeta_{m_k}^k(\boldsymbol{x})$, …. Then, the reduced basis functions $\{\zeta_l^k(\boldsymbol{x})\}_{l=1}^{m_k}$ have the following approximation property*

$$\frac{\sum_{q=1}^Q \left|\left|\tilde{\phi}_k^{loc}(\boldsymbol{x}, \omega_q) - \sum_{l=1}^{m_k} \left(\tilde{\phi}_k^{loc}(\boldsymbol{x}, \omega_q), \zeta_l^k(\boldsymbol{x})\right)_X \zeta_l^k(\boldsymbol{x})\right|\right|_X^2}{\sum_{q=1}^Q \left|\left|\tilde{\phi}_k^{loc}(\boldsymbol{x}, \omega_q)\right|\right|_X^2} = \frac{\sum_{s=m_k+1}^Q \lambda_s}{\sum_{s=1}^Q \lambda_s}, \tag{17}$$

where $X = L^2(D)$ or $X = H^1(D)$ and the number m_k is determined according to the ratio $\rho = \frac{\sum_{s=1}^{m_k} \lambda_s}{\sum_{s=1}^Q \lambda_s}$.

In practice, we choose the first m_k dominant reduced basis functions such that ρ is close enough to 1, in order to achieve a desired accuracy, say $\rho = 99\%$. More details of the POD method can be found in [6, 43]. Notice that reduced basis functions $\zeta_0^k(\mathbf{x})$ and $\zeta_l^k(\mathbf{x})$, $l = 1, \ldots, m_k$, approximately capture the mean profile and fluctuation of multiscale basis functions associated with $\mathbf{x}_k$, respectively. Thus, for each realization

of the random potential the associated multiscale basis functions can be approximated by the reduced basis functions, i.e.,

$$\phi_k^{\mathrm{loc}}(\mathbf{x},\omega) \approx \zeta_0^k(\mathbf{x}) + \sum_{l=1}^{m_k} c_l(\omega)\zeta_l^k(\mathbf{x}). \tag{18}$$

Remark 3.2. To construct the multiscale reduced basis functions, we partition the coarse grids D^k into fine-scale quadrilateral elements with grid size $h \ll \varepsilon$, which requires additional computational cost in the offline stage. However, the precomputed reduced basis functions can be used repeatedly to solve (1) for each realization of the random potential and different initial data, which results in considerable savings.

3.3. Estimation of the number of learning samples. We shall study the continuous dependence of multiscale basis functions on the random potential, which provide guidance on how to determine the number of samples in the construction of multiscale basis functions. For notational simplification, we carry out the analysis for multiscale basis functions without localization.

Let $\varphi_s^h(\mathbf{x})$, $s = 1, \ldots, N_h$, denote the finite element basis functions defined on a fine mesh with size h and N_h is the number of fine-scale finite element basis functions. When we numerically solve (4)–(5), we represent the multiscale basis function as $\phi_i(\mathbf{x}) = \sum_{s=1}^{N_h} c_s\varphi_s^h(\mathbf{x})$ and obtain the following quadratic programming problem with equality constraints,

$$\begin{cases} \min\limits_{\boldsymbol{c}} \dfrac{1}{2}\boldsymbol{c}^T G\boldsymbol{c} \\ \text{s.t. } A\boldsymbol{c} = \boldsymbol{b}, \end{cases} \tag{19}$$

where $\boldsymbol{c} = [c_1, \ldots, c_{N_h}]^T$ is the coefficients and G is a symmetric positive definite matrix on the fine triangulation $\mathcal{T}_h$ with the (i,j) component

$$G_{ij} = \frac{\varepsilon^2}{2}(\nabla\varphi_i^h, \nabla\varphi_j^h) + (v^\varepsilon(\mathbf{x},\omega_q)\varphi_i^h, \varphi_j^h). \tag{20}$$

In (19), A is an N_h-by-N_H matrix with $A_{ij} = (\varphi_i^h, \varphi_j^H)$ and $\boldsymbol{b}$ is an N_h-by-1 vector with only the ith entry being 1 and the others being 0.

The following result states the continuous dependence of multiscale basis functions on the random potential.

THEOREM 3.2. *Assume the random potential $v^\varepsilon(\boldsymbol{x},\omega)$ is almost surely bounded, i.e.,* (14) *is satisfied and the grid size of the fine-scale triangles is small such that* (1) *$h/\varepsilon = \kappa$ is small; and* (2) *$h^d\|v^\varepsilon(\cdot,\omega_1) - v^\varepsilon(\cdot,\omega_2)\|_{L^\infty(D)} < 1$. Then for two realizations ω_1 and ω_2 of the random potential $v^\varepsilon(\boldsymbol{x},\omega)$, the corresponding multiscale basis functions satisfy*

$$\|\phi(\cdot,\omega_1) - \phi(\cdot,\omega_2)\|_{L^\infty(D)} \le \frac{C}{\kappa^6}\varepsilon^{-2}\|v^\varepsilon(\cdot,\omega_1) - v^\varepsilon(\cdot,\omega_2)\|_{L^\infty(D)}, \tag{21}$$

where the constant C is independent of h, ε, and $\|v^\varepsilon(\cdot,\omega_1) - v^\varepsilon(\cdot,\omega_2)\|_{L^\infty(D)}$.

Proof. Under the assumptions that $v^\varepsilon(\mathbf{x},\omega)$ is almost surely bounded and $h/\varepsilon = \kappa$ is small, we know that G is a positive definite matrix. Moreover, we know that A has full rank, i.e., $\mathrm{rank}(A) = N_H$. Therefore, the quadratic optimization problem (19)

has a unique minimizer, satisfying the Karush–Kuhn–Tucker condition. Specifically, the unique minimizer of (19) is explicitly written as

$$\boldsymbol{c} = G^{-1}A^T(AG^{-1}A^T)^{-1}\boldsymbol{b}. \tag{22}$$

For two realizations ω_1 and ω_2, we define $\delta V = G_1 - G_2$. Then

$$(\delta V)_{ij} = \left((v(\cdot,\omega_1) - v(\cdot,\omega_2))\,\varphi_i^h, \varphi_j^h\right) \tag{23}$$

and, thus,

$$\|\delta V\|_\infty \le h^d \|v^\varepsilon(\cdot,\omega_1) - v^\varepsilon(\cdot,\omega_2)\|_{L^\infty(D)}. \tag{24}$$

We choose h to be small enough such that $\|\delta V\|_\infty \le 1$, and have

$$G_2^{-1} = \sum_{n=0}^{\infty} \left(G_1^{-1}\delta V\right)^n G_1^{-1}$$

and, thus,

$$\begin{aligned}
\boldsymbol{c}_2 - \boldsymbol{c}_1 &= \left[G_2^{-1} - G_1^{-1}\right] A^T(AG_1^{-1}A^T)^{-1}\boldsymbol{b} + G_2^{-1}A^T\left[(AG_2^{-1}A^T)^{-1} - (AG_1^{-1}A^T)^{-1}\right]\boldsymbol{b} \\
&= G_1^{-1}\delta V G_1^{-1}A^T(AG_1^{-1}A^T)^{-1}\boldsymbol{b} \\
&\quad - G_2^{-1}A^T(AG_1^{-1}A^T)^{-1}(AG_1^{-1}\delta V G_1^{-1}A^T)(AG_1^{-1}A^T)^{-1}\boldsymbol{b} + o(\|\delta V\|_\infty) \\
&= G_1^{-1}\delta V G_1^{-1}A^T(AG_1^{-1}A^T)^{-1}\boldsymbol{b} \\
&\quad - G_1^{-1}A^T(AG_1^{-1}A^T)^{-1}(AG_1^{-1}\delta V G_1^{-1}A^T)(AG_1^{-1}A^T)^{-1}\boldsymbol{b} + o(\|\delta V\|_\infty).
\end{aligned}$$

Therefore,

$$\begin{aligned}
|\boldsymbol{c}_2 - \boldsymbol{c}_1|_\infty \le C\|A\|_\infty \|G_1^{-1}\|_\infty^2 \|(AG_1^{-1}A^T)^{-1}\|_\infty |\boldsymbol{b}|_\infty \\
\times \left(1 + \|A\|_\infty^2 \|G_1^{-1}\|_\infty \|(AG_1^{-1}A^T)^{-1}\|_\infty\right)\|\delta V\|_\infty.
\end{aligned}$$

By their definitions, we have

$$\|A\|_\infty \le Ch^d, \quad |\boldsymbol{b}|_\infty = 1, \quad \|G_1^{-1}\|_\infty \le Ch^{-2}, \quad \|G_1\|_\infty \le C\max\{\varepsilon^2, h^2\} \le C\varepsilon^2$$

and, thus,

$$|\boldsymbol{c}_2 - \boldsymbol{c}_1|_\infty \le C\varepsilon^4 h^{-6} h^{-d}\|\delta V\|_\infty \le C\varepsilon^4 h^{-6}\|v^\varepsilon(\cdot,\omega_2) - v^\varepsilon(\cdot,\omega_1)\|_{L^\infty(D)}.$$

We complete the proof since $h/\varepsilon = \kappa$ and $\|\phi(\cdot,\omega_2) - \phi(\cdot,\omega_1)\|_{L^\infty(D)} \le |\boldsymbol{c}_2 - \boldsymbol{c}_1|_\infty$. ∎

Equipped with Theorem 3.2, we can estimate the number of samples in the construction of multiscale reduced basis functions. Suppose the random potential is of the form (16). For any $\delta > 0$, we choose an integer Q_δ and a set of random samples $\{v^\varepsilon(\mathbf{x},\omega_q)\}_{q=1}^{Q_\delta}$ such that

$$\mathbb{E}\left[\inf_{1\le q\le Q_\delta} \left|\left|v_m^\varepsilon(\mathbf{x},\omega) - v_m^\varepsilon(\mathbf{x},\omega_q)\right|\right|_{L^\infty(D)}\right] \le \delta, \tag{25}$$

where the expectation is taken over the random variables in $v_m^\varepsilon(\mathbf{x},\omega)$ of the form (16). We can give a way to choose the random samples $\{v^\varepsilon(\mathbf{x},\omega_q)\}_{q=1}^{Q_\delta}$ since the distribution of the random variables $\xi_i(\omega)$, $i = 1,\dots,m$, is known.

For every $\mathbf{x}_k \in \mathcal{N}$, let $\{\phi_k(\mathbf{x},\omega_q)\}_{q=1}^{Q_\delta}$ be the samples of multiscale basis functions associated with $\mathbf{x}_k$. Then, we have

$$\mathbb{E}\left[\inf_{1\le q\le Q_\delta} \left|\left|\phi_k(\mathbf{x},\omega)-\phi_k(\mathbf{x},\omega_q)\right|\right|_{L^\infty(D)}\right] \le \frac{C}{\kappa^6}\varepsilon^{-2}\delta. \tag{26}$$

Given parameters ε and h, we choose δ and Q_δ so that the right-hand side of (26) is small. Then, the space of multiscale basis functions can be well approximated by the samples of multiscale basis functions $\{\phi_k(\mathbf{x},\omega_q)\}_{q=1}^{Q_\delta}$ with controllable accuracy and the POD method is further applied to construct multiscale reduced basis functions.

3.4. Derivation of our method based on the multiscale reduced basis functions. In this section, we present our method for solving the random Schrödinger equation: in the physical space, we use the multiscale reduced basis functions obtained in section 3.2; in the random space, we use the qMC method.

The implementation of the qMC method is fairly easy. For instance, given a set of qMC samples, expectation of the solution is approximated by

$$\mathbb{E}\left[\psi^\varepsilon(t,\mathbf{x},\omega)\right] \approx \frac{1}{n}\sum_{i=1}^{n}\psi^\varepsilon(t,\mathbf{x},\omega_i), \tag{27}$$

where n is the number of qMC samples. Details of the generation of qMC samples and its convergence analysis will be discussed in section 4.

Now, we focus on how to approximate the wave function in the physical space for each qMC sample ω_s. For each node point $\mathbf{x}_k \in \mathcal{N}$, we have constructed a set of multiscale reduced basis functions $\{\zeta_i^k\}_{i=0}^{m_k}$ and represent the wave function by

$$\psi^\varepsilon(t,\mathbf{x},\omega_s) = \sum_{k=1}^{N_H}\sum_{l=0}^{m_k} c_l^k(t,\omega_s)\zeta_l^k(\mathbf{x}), \tag{28}$$

where m_k is the number of multiscale reduced basis functions associated with the node $\mathbf{x}_k$. In the Galerkin formulation, we have the following weak form,

$$\left(i\varepsilon\partial_t\sum_{k=1}^{N_H}\sum_{l=0}^{m_k} c_l^k(t,\omega_s)\zeta_l^k(\mathbf{x}),\zeta_r^j(\mathbf{x})\right) = \left(\mathcal{H}(\mathbf{x},\omega_s)\sum_{k=1}^{N_H}\sum_{l=0}^{m_k} c_l^k(t,\omega_s)\zeta_l^k(\mathbf{x}),\zeta_r^j(\mathbf{x})\right), \tag{29}$$
$$\mathbf{x}\in D,\quad t\in\mathbb{R},\quad j=1,\dots,N_H,\quad r=0,\dots,m_k,$$

where $\mathcal{H}(\mathbf{x},\omega_s)$ is a deterministic operator. To numerically solve (29), we introduce some notations. Let S, M, and $V(\omega_s)$ be matrices with dimension $\sum_{k=1}^{N_H}(m_k+1)\times\sum_{k=1}^{N_H}(m_k+1)$. Their entries are given by

$$S_{\sum_{i=1}^{k}(m_i+1)+l,\ \sum_{i=1}^{j}(m_i+1)+r} = \int_D \nabla\zeta_l^k\cdot\nabla\zeta_r^j \mathrm{d}\mathbf{x},$$
$$M_{\sum_{i=1}^{k}(m_i+1)+l,\ \sum_{i=1}^{j}(m_i+1)+r} = \int_D \zeta_l^k\zeta_r^j \mathrm{d}\mathbf{x},$$
$$V_{\sum_{i=1}^{k}(m_i+1)+l,\ \sum_{i=1}^{j}(m_i+1)+r}(\omega_s) = \int_D \zeta_l^k v^\varepsilon(\mathbf{x},\omega_s)\zeta_r^j \mathrm{d}\mathbf{x}.$$

Then, we can reduce the weak formulation (29) into the following ODE system

$$i\varepsilon M\frac{\mathrm{d}\mathbf{c}(t,\omega_s)}{\mathrm{d}t} = \left(\frac{\varepsilon^2}{2}S+V(\omega_s)\right)\mathbf{c}(t,\omega_s), \tag{30}$$

where the column vector

$$\mathbf{c}(t,\omega_s) = (c_0^1(t,\omega_s),\dots,c_{m_1}^1(t,\omega_s),\dots,c_0^{N_H}(t,\omega_s),\dots,c_{m_{N_H}}^{N_H}(t,\omega_s))^T$$

consists of all expansion coefficients of the solution $\psi^\varepsilon(t,\mathbf{x},\omega_s)$ onto multiscale reduced basis functions. We can further rewrite (30) as

$$\frac{d\mathbf{c}(t,\omega_s)}{dt} = \frac{1}{i\varepsilon}B(\omega_s)\mathbf{c}(t,\omega_s), \tag{31}$$

where $B(\omega_s) = M^{-1}A(\omega_s)$ and $A(\omega_s) = \frac{\varepsilon^2}{2}S + V(\omega_s)$.

Thanks to the spatial reduction of multiscale reduced basis functions, the degrees of freedom in the column vector $\mathbf{c}(t,\omega_s)$ is much smaller than that of a brute-force finite element solver. In practice, we first compute the eigendecomposition or Jordan canonical form of $B(\omega_s)$ and then solve the above ODE system (31) explicitly. Therefore, we can directly obtain $\mathbf{c}(t,\omega_s)$ at any time without choosing temporal step size. Of course, multiscale basis functions constructed here can be incorporated with ODE solvers, such as the backward Euler method and the Crank–Nicolson method, where the temporal step size shall be chosen carefully to compromise stability and accuracy. More details can be found in [10].

Before ending this section, we shall explain why we choose the qMC method to approximate the random space of the electron wave function. Since the parameterization of a random potential may have high dimension, i.e., m is large in (15), nonintrusive methods, such as the sparse grid method [7] and the stochastic collocation method [38], become prohibitively expensive to solve PDEs with random coefficients. Polynomial chaos expansion (PCE) methods [21, 46] are also frequently used in the literature to solve PDEs with random coefficients. This type of method is very efficient if the solution is sufficiently smooth in the random space with small dimensionality. It also, however, suffers from the curse of dimensionality. The performance of the MC method does not depend on the dimension of the random space. However, its convergence rate is merely $O(\frac{1}{\sqrt{n}})$. The convergence rate of the qMC method is better both theoretically and numerically; see (46) in Theorem 4.5. Therefore, we choose the qMC method and its implementation is almost the same as the MC method.

4. Convergence analysis.

We shall analyze the approximation error of the proposed method, where the emphasis is put on computing functionals of the wave function.

4.1. Regularity of the wave function with respect to the random variables.

Since the potential $v^\varepsilon(\mathbf{x},\omega)$ in (1) is parameterized by m random variables $\xi_i(\omega)$, $i = 1,\dots,m$, in (16), i.e., $v_m^\varepsilon(\mathbf{x},\omega) = v^\varepsilon(\mathbf{x},\xi_1(\omega),\dots,\xi_m(\omega))$. The wave function $\psi_m^\varepsilon(t,\mathbf{x},\omega)$ satisfies

$$\begin{cases} i\varepsilon\partial_t\psi_m^\varepsilon = -\dfrac{\varepsilon^2}{2}\Delta\psi_m^\varepsilon + v_m^\varepsilon(\mathbf{x},\omega)\psi_m^\varepsilon, \quad \mathbf{x}\in D, \quad t\in\mathbb{R}, \\ \psi_m^\varepsilon \in H_{\mathrm{P}}^1(D), \\ \psi_m^\varepsilon|_{t=0} = \psi_{\mathrm{in}}(\mathbf{x}). \end{cases} \tag{32}$$

The Doob–Dynkin's lemma implies the wave function $\psi_m^\varepsilon(t,\mathbf{x},\omega)$ in (32) can also be represented by a functional of these random variables, i.e.,

$$\psi_m^\varepsilon(t,\mathbf{x},\omega) = \psi_m^\varepsilon(t,\mathbf{x},\xi_1(\omega),\dots,\xi_m(\omega)).$$

First of all, we analyze the error introduced by the parameterization of the random potential. We have the following estimate result.

LEMMA 4.1. *The difference between wave functions to* (32) *and* (1) *satisfies*

$$\|\psi_m^\varepsilon - \psi^\varepsilon\|_{L^2(\Omega,D)} \le \frac{T}{\varepsilon}\|v_m^\varepsilon - v^\varepsilon\|_{L^\infty(\Omega,D)} \quad \forall t \in [0,T]. \tag{33}$$

Proof. The difference $\delta\psi = \psi_m^\varepsilon - \psi^\varepsilon$ satisfies

$$\begin{cases} i\varepsilon\partial_t\delta\psi = -\dfrac{\varepsilon^2}{2}\Delta\delta\psi + v_m^\varepsilon\delta\psi + (v_m^\varepsilon - v^\varepsilon)\psi^\varepsilon, \quad \mathbf{x}\in D, \quad t\in\mathbb{R}, \\ \quad \delta\psi \in H_{\mathrm{P}}^1(D), \\ \delta\psi|_{t=0} = 0. \end{cases}$$

By a direct calculation, we have

$$\frac{\mathrm{d}}{\mathrm{d}t}\|\delta\psi\|_{L^2(\Omega,D)}^2 = \frac{1}{i\varepsilon}\int_\Omega\int_D \left(\overline{\delta\psi}(v_m^\varepsilon - v^\varepsilon)\psi^\varepsilon - \overline{\psi^\varepsilon}(v_m^\varepsilon - v^\varepsilon)\delta\psi\right)\mathrm{d}\mathbf{x}\mathrm{d}\rho(\omega),$$

where $\rho(\omega)$ is the probability measure induced by the randomness in the potential (16) and thus

$$\begin{aligned} \frac{\mathrm{d}}{\mathrm{d}t}\|\delta\psi\|_{L^2(\Omega,D)}^2 &\le \frac{2}{\varepsilon}\int_\Omega\int_D |\overline{\delta\psi}(v_m^\varepsilon - v^\varepsilon)\psi^\varepsilon|\mathrm{d}\mathbf{x}\mathrm{d}\rho(\omega) \\ &\le \frac{2}{\varepsilon}\int_\Omega \|\overline{\delta\psi}\|_{L^2(D)}\|v_m^\varepsilon - v^\varepsilon)\psi^\varepsilon\|_{L^2(D)}\mathrm{d}\rho(\omega) \\ &\le \frac{2}{\varepsilon}\int_\Omega \|\delta\psi\|_{L^2(D)}\|v_m^\varepsilon - v^\varepsilon\|_{L^\infty(D)}\mathrm{d}\rho(\omega) \\ &\le \frac{2\|v_m^\varepsilon - v^\varepsilon\|_{L^\infty(D,\Omega)}}{\varepsilon}\|\delta\psi\|_{L^2(D,\Omega)}. \end{aligned}$$

Therefore, we obtain

$$\|\delta\psi\|_{L^2(\Omega,D)} \le \frac{T}{\varepsilon}\|v_m^\varepsilon - v^\varepsilon\|_{L^\infty(\Omega,D)} \quad \forall t\in[0,T],$$

which completes the proof. ∎

To carry out error analysis for the qMC method, it is crucial to bound the mixed first derivatives of ψ_m^ε with respect to $\xi_i(\omega)$. Denote $\boldsymbol{\xi}(\omega) = (\xi_1(\omega),\ldots,\xi_m(\omega))^T$ for convenience. Let $\boldsymbol{\nu} = (\nu_1,\ldots,\nu_m)$ denote a multi-index of nonnegative integers, with $|\boldsymbol{\nu}| = \sum_{j=1}^m \nu_j$ and $|\boldsymbol{\nu}|_\infty = \max_{1\le j\le m}\nu_j$. The value of ν_j determines the number of derivatives to be taken with respect to ξ_j, and $\partial^{\boldsymbol{\nu}}\psi_m^\varepsilon$ denotes the mixed derivative of ψ_m^ε with respect to all variables specified by the multi-index $\boldsymbol{\nu}$.

LEMMA 4.2. *For any $\omega\in\Omega$, any time T, and for any multi-index $\boldsymbol{\nu}$ with $|\boldsymbol{\nu}| < \infty$, the partial derivative of $\psi_m^\varepsilon(t,\boldsymbol{x},\omega)$ satisfies the following a priori estimate:*

$$\|\partial^{\boldsymbol{\nu}}\psi_m^\varepsilon(t,\cdot,\omega)\|_{L^2(D)} \le \frac{|\boldsymbol{\nu}|!\,T^{|\boldsymbol{\nu}|}}{\varepsilon^{|\boldsymbol{\nu}|}}\left\{\prod_{j\ge1}\left(\sqrt{\lambda_j}\|v_j\|_{C^0(\bar{D})}\right)^{\nu_j}\right\} \quad \forall\, t\in[0,T]. \tag{34}$$

Proof. When $|\boldsymbol{\nu}| = 1$, we take the derivative of (32) with respect to $\xi_j(\omega)$. Let $\partial_j \psi_m = \partial_{\xi_j} \psi_m^\varepsilon$ and $\partial_j v_m = \partial_{\xi_j} v_m^\varepsilon$, we have

$$i\varepsilon \left(\partial_j \psi_m\right)_t = -\frac{\varepsilon^2}{2} \Delta \left(\partial_j \psi_m\right) + \left(\partial_j v_m\right) \psi_m^\varepsilon + v_m^\varepsilon \left(\partial_j \psi_m\right).$$

Thereafter, we have the following estimate by a direction calculation,

$$\begin{aligned}
\frac{\mathrm{d}}{\mathrm{d}t} \|\partial_j \psi_m\|_{L^2(D)}^2 &= \int_D \left\{ \left(\overline{\partial_j \psi_m}\right)_t \left(\partial_j \psi_m\right) + \left(\overline{\partial_j \psi_m}\right) \left(\partial_j \psi_m\right)_t \right\} \mathrm{d}\mathbf{x} \\
&= \int_D \left(-\frac{1}{i\varepsilon} \left(\partial_j v_m\right) \overline{\psi_m^\varepsilon} \left(\partial_j \psi_m\right) + \frac{1}{i\varepsilon} \left(\overline{\partial_j \psi_m}\right) \left(\partial_j v\right) \psi_m^\varepsilon \right) \mathrm{d}\mathbf{x} \\
&\le \frac{2}{\varepsilon} \|\partial_j \psi_m\|_{L^2(D)} \|\partial_j v \psi_m^\varepsilon\|_{L^2(D)} \le \frac{2}{\varepsilon} \|\partial_j \psi_m\|_{L^2(D)} \|\partial_j v_m\|_{L^\infty(D)}
\end{aligned}$$

and

$$\|\partial_j \psi_m\|_{L^2(D)} \le \frac{T}{\varepsilon} \|\partial_j v_m\|_{L^\infty(D)} \le \frac{T}{\varepsilon} \sqrt{\lambda_j} \|\phi_j\|_{C^0(\bar{D})}. \tag{35}$$

When $|\boldsymbol{\nu}| \ge 2$, we have

$$i\varepsilon \left(\partial^{\boldsymbol{\nu}} \psi_m\right)_t = -\frac{\varepsilon^2}{2} \Delta \left(\partial^{\boldsymbol{\nu}} \psi_m\right) + \sum_{\substack{\boldsymbol{\mu} \preceq \boldsymbol{\nu} \\ \boldsymbol{\mu} \ne \boldsymbol{\nu}}} \binom{\boldsymbol{\nu}}{\boldsymbol{\mu}} \left(\partial^{\boldsymbol{\nu}-\boldsymbol{\mu}} v_m\right) \left(\partial^{\boldsymbol{\mu}} \psi_m\right) + v_m^\varepsilon \left(\partial^{\boldsymbol{\nu}} \psi_m\right).$$

According to the definition of the random potential (15), we have $\partial^{\boldsymbol{\nu}-\boldsymbol{\mu}} v_m^\varepsilon = 0$ if $|\boldsymbol{\nu} - \boldsymbol{\mu}| \ge 2$. Thus, the above equation can be simplified as

$$i\varepsilon \left(\partial^{\boldsymbol{\nu}} \psi_m\right)_t = -\frac{\varepsilon^2}{2} \Delta \left(\partial^{\boldsymbol{\nu}} \psi_m\right) + \sum_{|\boldsymbol{\nu}-\boldsymbol{\mu}|=1} \binom{|\boldsymbol{\nu}|}{1} \left(\partial^{\boldsymbol{\nu}-\boldsymbol{\mu}} v_m\right) \left(\partial^{\boldsymbol{\mu}} \psi_m\right) + v_m^\varepsilon \left(\partial^{\boldsymbol{\nu}} \psi_m\right).$$

Similarly, we obtain

$$\begin{aligned}
&\frac{\mathrm{d}}{\mathrm{d}t} \|\partial^{\boldsymbol{\nu}} \psi_m\|_{L^2(D)}^2 \\
&= \int_D \left\{ \left(\overline{\partial^{\boldsymbol{\nu}} \psi_m}\right)_t \left(\partial^{\boldsymbol{\nu}} \psi_m\right) + \left(\overline{\partial^{\boldsymbol{\nu}} \psi_m}\right) \left(\partial^{\boldsymbol{\nu}} \psi_m\right)_t \right\} \mathrm{d}\mathbf{x} \\
&= \sum_{|\boldsymbol{\nu}-\boldsymbol{\mu}|=1} \binom{|\boldsymbol{\nu}|}{1} \int_D \left(-\frac{1}{i\varepsilon} \left(\partial^{\boldsymbol{\nu}-\boldsymbol{\mu}} v_m\right) \overline{\left(\partial^{\boldsymbol{\mu}} \psi_m\right)} \left(\partial^{\boldsymbol{\nu}} \psi_m\right) + \frac{1}{i\varepsilon} \left(\overline{\partial^{\boldsymbol{\nu}} \psi_m}\right) \left(\partial^{\boldsymbol{\nu}-\boldsymbol{\mu}} v_m\right) \left(\partial^{\boldsymbol{\mu}} \psi_m\right) \right) \mathrm{d}\mathbf{x} \\
&\le \frac{2|\boldsymbol{\nu}|}{\varepsilon} \|\partial^{\boldsymbol{\nu}} \psi_m\|_{L^2(D)} \sum_{|\boldsymbol{\nu}-\boldsymbol{\mu}|=1} \|\left(\partial^{\boldsymbol{\nu}-\boldsymbol{\mu}} v_m\right)\|_{L^\infty(D)} \|\left(\partial^{\boldsymbol{\mu}} \psi_m\right)\|_{L^2(D)}
\end{aligned} \tag{36}$$

and

$$\|\partial^{\boldsymbol{\nu}} \psi_m\|_{L^2(D)} \le \frac{T|\boldsymbol{\nu}|}{\varepsilon} \sum_{|\boldsymbol{\nu}-\boldsymbol{\mu}|=1} \|\left(\partial^{\boldsymbol{\nu}-\boldsymbol{\mu}} v_m\right)\|_{L^\infty(D)} \|\left(\partial^{\boldsymbol{\mu}} \psi_m\right)\|_{L^2(D)}. \tag{37}$$

Now we are ready to prove the theorem by mathematical induction. From (35), we know that (34) holds for $|\boldsymbol{\nu}| = 1$. Assume that (34) holds for $\boldsymbol{\mu}$ with $|\boldsymbol{\nu} - \boldsymbol{\mu}| = 1$. Substituting this into (37) yields the desired estimate for the $\boldsymbol{\nu}$ case. ∎

Remark 4.1. The above derivation is similar to that in [27], where an estimate in the $L^2(D, \Omega)$ norm is obtained. Here, for each random realization ω, we have the estimate (34) in the $L^2(D)$ norm, which will be used to prove the convergence in qMC.

4.2. Main result of the error analysis. In the framework of uncertainty quantification, we are interested in computing some statistical quantities of the electron wave function. As such, we shall present the error analysis of our method in computing functionals of ψ_m^ε.

Let $\mathcal{G}(\cdot)$ be a continuous linear functional on $L^2(D)$, then there exists a constant $C_\mathcal{G}$ such that

$$|\mathcal{G}(u)| \le C_\mathcal{G}\|u\|_{L^2(D)}$$

for all $u \in L^2(D)$. Consider the following integral

$$I_m(F) = \int_{\boldsymbol{\xi}\in[0,1]^m} F(\boldsymbol{\xi})\mathrm{d}\boldsymbol{\xi} \tag{38}$$

with $F(\boldsymbol{\xi}) = \mathcal{G}(\psi_m^\varepsilon(\cdot,\boldsymbol{\xi}))$. We approximate the integral over the unit cube by randomly shifted lattice rules

$$Q_{m,n}(\boldsymbol{\Delta}; F) \triangleq \frac{1}{n}\sum_{i=1}^{n} F\left(\mathrm{frac}\left(\frac{i\boldsymbol{z}}{n} + \boldsymbol{\Delta}\right)\right),$$

where $\boldsymbol{z} \in \mathbb{N}^m$ is the (deterministic) generating vector and $\boldsymbol{\Delta} \in [0,1]^m$ is the random shift which is uniformly distributed over $[0,1]^m$. Notice that m is the dimension of the random vector $\boldsymbol{\xi}$ in the random potential and n is the number of the sample point in implementing the qMC method. The interested reader is referred to [13] for more details of the randomly shifted lattice rules in the qMC method.

LEMMA 4.3. *Let F be the integrand in (38). Given $m, n \in \mathbb{N}$ with $n \le 10^{30}$, weights $\boldsymbol{\gamma} = (\gamma_\mathbf{u})_{\mathbf{u}\subset\mathbb{N}}$, a randomly shifted lattice rule with n points in m dimensions can be constructed by a component-by-component algorithm such that, for all $\lambda \in (1/2, 1]$,*

$$\sqrt{\mathbb{E}^{\boldsymbol{\Delta}}|I_m(F) - Q_{m,n}(\cdot;F)|^2} \le 9C^* C_{\boldsymbol{\gamma},m}(\lambda) n^{-1/(2\lambda)} \tag{39}$$

with

$$C_{\boldsymbol{\gamma},m}(\lambda) = \left(\sum_{\emptyset\neq\mathbf{u}\subseteq\{1:m\}} \gamma_\mathbf{u}^\lambda \prod_{j\in\mathbf{u}} \varrho(\lambda)\right)^{1/(2\lambda)} \left(\sum_{\mathbf{u}\subseteq\{1:m\}} \frac{(|\mathbf{u}|!)^2 T^{2|\mathbf{u}|}}{\gamma_\mathbf{u}\varepsilon^{2|\mathbf{u}|}} \prod_{j\in\mathbf{u}} \lambda_j \|\phi_j\|^2_{C^0(\bar{D})}\right)^{1/2}. \tag{40}$$

Proof. The proof of this result is essentially an application of the Koksma–Hlawka inequality, which is the same as the proofs of Theorems 15, 16, and 17 in [22], or Theorem 5.10 in [13] with the following modification of estimates:

$$\varrho(\lambda) = 2\left(\frac{\sqrt{2\pi}}{\pi^{2-2\eta_*}(1-\eta_*)\eta_*}\right)^\lambda \zeta\left(\lambda + \frac{1}{2}\right), \quad \eta_* = \frac{2\lambda-1}{4\lambda}, \tag{41}$$

with $\zeta(x) = \sum_{j=1}^\infty j^{-x}$ the Riemann zeta function, and $C^* = \|\mathcal{G}\|_{L^2(D)}$. ∎

To analyze the error of our method, we need to make some assumptions on the regularity of the eigenfunctions and the decay rate of the eigenvalues in the KL expansion (16) of the random potential.

Assumption 4.4.

(a) There exist $C > 0$ and $\Theta > 1$ such that $\lambda_j \le Cj^{-\Theta}$ for $j \ge 1$.

(b) The KL eigenfunctions $v_j(\mathbf{x})$ are continuous and there exist $C > 0$ and $\eta \in [0, \frac{\Theta-1}{2\Theta})$ such that $\|v_j\|_{C^0(\bar{D})} \le C\lambda_j^{-\eta}$ for $j \ge 1$.

(c) The sequence defined by $\sqrt{\lambda_j}\|v_j\|_{C^0(\bar{D})}$, $j \ge 1$, satisfies

$$\sum_{j\ge1}(\sqrt{\lambda_j}\|v_j\|_{C^0(\bar{D})})^p < \infty$$

for some $p \in (0, 1]$, and $\sum_{j\ge1}\sqrt{\lambda_j}\|v_j\|_{C^0(\bar{D})} < \frac{\varepsilon}{T}\sqrt{\varrho(\lambda)}$ for $\lambda \in (1/2, 1]$.

Recall that ψ^ε and ψ^ε_m are solutions to (1) and (32), respectively. Denote by $\psi^\varepsilon_{H,m}$ the solution obtained by our method using the multiscale reduced basis functions in the physical space and the qMC method in the random space. Under Assumption 4.4 for the random potential, we have the following error estimate.

THEOREM 4.5. *Consider the approximation of $\mathbb{E}[\mathcal{G}(\psi^\varepsilon)]$ via the qMC multiscale FEM, denoted by $Q_{m,n}(\cdot; \mathcal{G}(\psi^\varepsilon_{H,m}))$, where we assume $\psi^\varepsilon \in L^2(\Omega; H^2(D))$. A randomly shifted lattice rule $Q_{m,n}$ is applied to $\mathcal{G}(\psi^\varepsilon_m)$. Then, we can bound the root-mean-square error with respect to the uniformly distributed shift $\mathbf{\Delta} \in [0, 1]^m$ by*

(42)
$$\sqrt{\mathbb{E}^{\mathbf{\Delta}}\left[\left(\mathbb{E}[\mathcal{G}(\psi^\varepsilon)] - Q_{m,n}(\cdot; \mathcal{G}(\psi^\varepsilon_{H,m}))\right)^2\right]} \le C\left(\frac{H^2}{\varepsilon^2} + \frac{m^{-\chi}}{\varepsilon} + n^{-r}\right), \quad 0 < t \le T,$$

for $0 < \chi \le (1/2 - \eta)\Theta - 1/2$, and with $r = 1/p - 1/2$ for $p \in (2/3, 1]$ and $r = 1 - \delta$ for $p \le 2/3$, with δ arbitrarily small. Here the constant C is independent of ε, m, and n but depends on T.

Proof. The linearity of operator $\mathcal{G}$ implies

$$\mathcal{G}(\psi^\varepsilon) - \mathcal{G}(\psi^\varepsilon_{H,m}) = \mathcal{G}(\psi^\varepsilon) - \mathcal{G}(\psi^\varepsilon_H) + \mathcal{G}(\psi^\varepsilon_H) - \mathcal{G}(\psi^\varepsilon_{H,m}). \tag{43}$$

Under the assumption $\psi^\varepsilon \in L^2(\Omega; H^2(D))$, we have (see, for example, [9]),

$$|\mathbb{E}[\mathcal{G}(\psi^\varepsilon) - \mathcal{G}(\psi^\varepsilon_H)]| \le C\frac{H^2}{\varepsilon^2}. \tag{44}$$

Under assumptions (b) and (c) in Assumption 4.4, we have, based on Lemma 4.1,

$$|\mathcal{G}(\psi^\varepsilon_H) - \mathcal{G}(\psi^\varepsilon_{H,m})| \le C\frac{m^{-\chi}}{\varepsilon} \tag{45}$$

for all $0 < \chi \le (1/2 - \eta)\Theta - 1/2$. Detailed derivation is essentially the same as the proof of Theorem 8 in [22].

Finally, when applying the qMC method to (43), we need to analyze the error in the qMC method. We adopt the standard framework, i.e., the Koksma–Hlawka inequality. Under Assumption 4.4, we have, based on Lemmas 4.2 and 4.3,

$$\sqrt{\mathbb{E}^{\mathbf{\Delta}}|I_m(F) - Q_{m,n}(\cdot; F)|^2} \le Cn^{-r}, \tag{46}$$

where $r = 1/p - 1/2$ for $p \in (2/3, 1]$ and $r = 1 - \delta$ for $p \le 2/3$, with δ arbitrarily small. Detailed derivation is essentially the same as the proof of Theorem 20 in [22]. A combination of the above estimates completes the proof. ∎

Remark 4.2. The term $\frac{m^{-\chi}}{\varepsilon}$ in the error estimate (42) can be viewed as a modeling error. When the m-term KL truncation potential $v^\varepsilon_m(\mathbf{x}, \omega)$ in (16) provides an accurate approximation to the potential $v^\varepsilon(\mathbf{x}, \omega)$, the term $\frac{m^{-\chi}}{\varepsilon}$ becomes small or negligible.

Remark 4.3. In section 5, we will show that the proposed method works well for a large class of random potentials, even when the eigenvalues in the KL expansion have a relatively slow decay rate. Therefore, Assumption 4.4 is a rather technical assumption for the convergence analysis of the proposed method.

Remark 4.4. In the error analysis for the qMC method, we assume $\boldsymbol{\xi} = (\xi_1, \ldots, \xi_m) \in [0,1]^m$ for notational convenience; see (38), where ξ_i are i.i.d. uniform random variables. In the KL expansion (16) representation for $v_m^\varepsilon(\mathbf{x}, \omega)$, we choose $\xi_i \in [-\sqrt{3}, \sqrt{3}]$, $i = 1, \ldots, m$, so that the conditions $\mathbb{E}[\xi_i] = 0$, $\mathbb{E}[\xi_i \xi_j] = \delta_{ij}$ are satisfied. The same convergence result can be obtained with little modification of the current proof.

5. Numerical examples. In this section, we conduct numerical experiments to test the accuracy and the efficiency of our method. Specifically, we will present convergence tests with respect to the physical grid size, the number of multiscale reduced basis functions, and the number of qMC samples. In addition, we will investigate the existence of Anderson localization in both 1 dimension and 2 dimensions. For convenience, we first introduce the L^2 norm and H^1 norm as

$$||\psi^\varepsilon||_{L^2}^2 = \int_D |\psi^\varepsilon|^2 \mathrm{d}\mathbf{x}, \quad ||\psi^\varepsilon||_{H^1}^2 = \int_D |\nabla \psi^\varepsilon|^2 \mathrm{d}\mathbf{x} + \int_D |\psi^\varepsilon|^2 \mathrm{d}\mathbf{x}.$$

In what follows, we compare the relative error between expectations of the numerical solution $\psi_{\mathrm{num}}^\varepsilon$ and the reference solution $\psi_{\mathrm{ref}}^\varepsilon$ in both the L^2 norm and H^1 norms:

$$\mathrm{Error}_{L^2} = \frac{||\mathbb{E}[\psi_{\mathrm{num}}^\varepsilon] - \mathbb{E}[\psi_{\mathrm{ref}}^\varepsilon]||_{L^2}}{||\mathbb{E}[\psi_{\mathrm{ref}}^\varepsilon]||_{L^2}},$$
$$\mathrm{Error}_{H^1} = \frac{||\mathbb{E}[\psi_{\mathrm{num}}^\varepsilon] - \mathbb{E}[\psi_{\mathrm{ref}}^\varepsilon]||_{H^1}}{||\mathbb{E}[\psi_{\mathrm{ref}}^\varepsilon]||_{H^1}}.$$

Here $\mathbb{E}[\psi_{\mathrm{num}}^\varepsilon] = \int_\Omega \psi_{\mathrm{num}}^\varepsilon(t, \mathbf{x}, \omega) \mathrm{d}\rho(\omega)$, $\mathbb{E}[\psi_{\mathrm{ref}}^\varepsilon] = \int_\Omega \psi_{\mathrm{ref}}^\varepsilon(t, \mathbf{x}, \omega) \mathrm{d}\rho(\omega)$, Ω is the random space, and $\rho(\omega)$ is the probability measure induced by the randomness in (16). The reference solution refers to the numerical wave function using a very fine mesh and a large amount of qMC samples. In numerical experiments, we use the MATLAB Statistics Toolbox to generate the Sobol sequence to implement the qMC method. When we use the POD method to construct multiscale reduced basis functions, we observed similar decay behaviors of the associated eigenvalues at each coarse grid point. Therefore, we choose the same reduced basis number m_k for all the coarse grid points.

5.1. Convergence in the physical space. Consider the 1D Schrödinger equation over $D = [-\pi, \pi]$,

$$i\varepsilon \partial_t \psi^\varepsilon = -\frac{\varepsilon^2}{2} \partial_{xx} \psi^\varepsilon + v^\varepsilon(x, \omega) \psi^\varepsilon, \tag{47}$$

where the periodic condition is imposed, the initial data $\psi_{\mathrm{in}}(x) = (\frac{10}{\pi})^{1/4} e^{-20(x-0)^2}$, and the random potential $v^\varepsilon(x, \omega)$ is defined as

$$v^\varepsilon(x, \omega) = 1 + \sigma \sum_{j=1}^{3} \sin(jx^2) \sin\left(\frac{x}{E_j}\right) \xi_j(\omega). \tag{48}$$

In the random potential (48), σ is used to control the strength of the random potential, and $\xi_j(\omega)$'s are mean-zero and independent random variables uniformly distributed

TABLE 1
Relative L^2 and H^1 errors for the expectation of the wave function when $\varepsilon = 1/16$.

H	Error$_{L^2}$	Order	Error$_{H^1}$	Order
$2\pi/32$	0.09862312		0.32096262	
$2\pi/64$	0.00129644	6.25	0.01449534	4.47
$2\pi/128$	0.00002892	5.49	0.00076150	4.25
$2\pi/256$	0.00000950	1.61	0.00014161	2.42

in $[-\sqrt{3}, \sqrt{3}]$. Moreover, we choose $\varepsilon = \frac{1}{16}$, $\sigma = 1$, and $E = [\frac{1}{9}, \frac{1}{13}, \frac{1}{11}]$, i.e., the characteristic length scale of randomness is different from the semiclassical parameter.

Convergence with respect to the coarse grid size H. In our numerical test, we set the final computational time $T = 1$. For the reference solution, we choose the fine mesh to be $h = \frac{2\pi}{2048}$ and the qMC sample number to be $n = 16000$. For our method, we choose the POD modes $m_k = 3$, the sampling number in the offline training stage to be 200, and the number of qMC samples in the online stage to be 2560.

In Table 1, we compute the relative errors of the expectation of the wave function in both the L^2 norm and H^1 norms for a series of coarse meshes with grid size ranging from $H = \frac{2\pi}{32}$ to $H = \frac{2\pi}{256}$. A nice convergence in the physical space is observed. It is worth mentioning that the numerical rate of convergence is higher than that in (44). We attribute the discrepancy to three reasons: (1) the reference solution for comparison is calculated by the standard FEM method on a fine mesh; (2) sampling errors exist in all quantities for comparison; (3) the convergence analysis relies on the regularity of the wave function with respect to the spatial variables while the regularity in numerical examples is typically higher.

Verification of the exponential decay of multiscale basis functions. For the same problem as above, we choose four different realizations of the multiscale basis functions centered at $x = 0$, i.e., $\phi(x, \boldsymbol{\xi}(\omega_i))$, $i = 1, 2, 3, 4$, which are generated in the offline training stage of our previous experiment when $H = \frac{2\pi}{256}$. In Figure 1(a), we plot $|\nabla\phi(x, \boldsymbol{\xi}(\omega_i))|/||\nabla\phi(x, \boldsymbol{\xi}(\omega_i))||_{L_2(D)}$, $i = 1, 2, 3, 4$. In Figure 1(b), we plot the quantity $E_{\text{relative}} = \frac{||\nabla\phi(x,\boldsymbol{\xi}(\omega_i))||_{L_2(D)} - ||\nabla\phi(x,\boldsymbol{\xi}(\omega_i))||_{L_2(D_\ell)}}{\max(||\nabla\phi(x,\boldsymbol{\xi}(\omega_i))||_{L_2(D)} - ||\nabla\phi(x,\boldsymbol{\xi}(\omega_i))||_{L_2(D_\ell)})}$ with respect to the patch size ℓ (defined in (7)), which shows the decay rate of E_{relative} with respect to ℓ.

One can see that each realization of the multiscale basis functions decays exponentially fast away from the center $x = 0$. Since the multiscale basis functions have an exponential decay property, the approximated multiscale basis using the reduced basis functions (see (18)) still has the same property.

Convergence with respect to the number of multiscale reduced basis functions. We study how the approximation error depends on the number of multiscale reduced bases used at each coarse mesh node $\mathbf{x}_k$, i.e., changing the POD modes m_k. Again, we solve (47)–(48) when $\varepsilon = \frac{1}{16}$, $\sigma = 1$, and $E = [\frac{1}{9}, \frac{1}{13}, \frac{1}{11}]$. The final computational time $T = 1$. For the reference solution, we choose the grid size to be $h = \frac{2\pi}{2048}$ and the number of qMC samples to be $n = 16000$. For our method, we choose the number of samples in the offline training stage to be 200 and the number of qMC samples in the online stage to be 2560. We fix the coarse grid size $H = \frac{2\pi}{128}$ and record the relative errors as a function of the number of multiscale reduced basis functions.

In Figure 2, we plot the relative L^2 and H^1 errors with respect to the number of multiscale reduced basis functions. It is observed when $m_k = 2$ or $m_k = 3$ that results have already been good enough in the sense that relative errors are less than

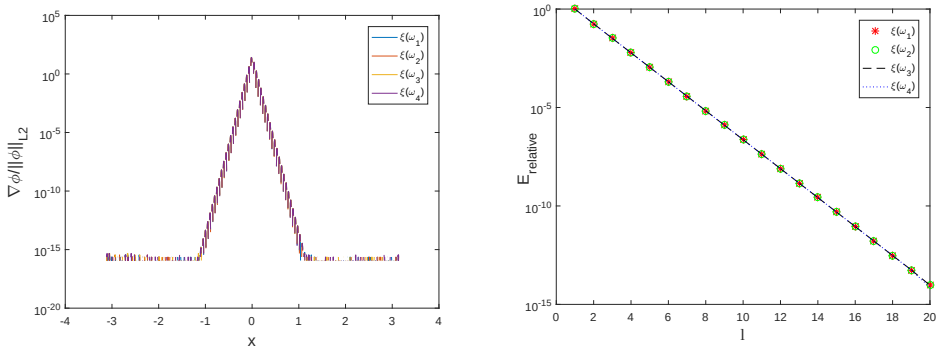

(a) $\nabla\phi/||\phi||_{L_2}$ with respect to the distance to $x = 0$.

(b) $E_{\text{relative}} = \frac{||\nabla\phi(x,\xi(\omega_i))||_{L_2(D)} - ||\nabla\phi(x,\xi(\omega_i))||_{L_2(D_\ell)}}{\max(||\nabla\phi(x,\xi(\omega_i))||_{L_2(D)} - ||\nabla\phi(x,\xi(\omega_i))||_{L_2(D_\ell)})}$.

FIG. 1. *Exponentially decaying properties of the multiscale basis functions for four different realizations.*

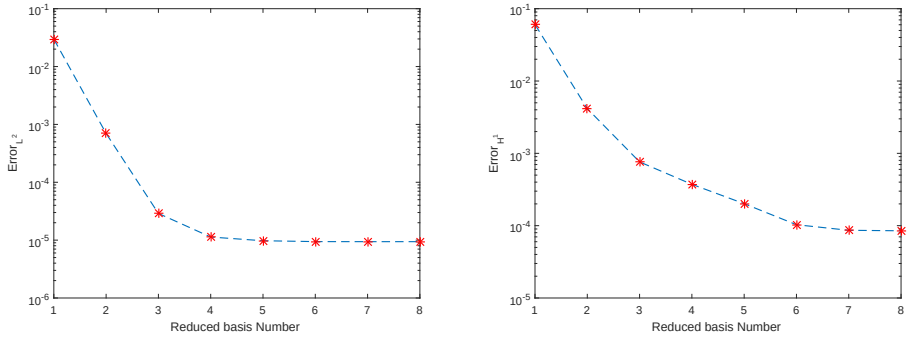

(a) Relative error in L^2 norm.

(b) Relative error in H^1 norm.

FIG. 2. *Relative errors with respect to the number of the multiscale reduced basis functions.*

1%. These numerical results indicate that multiscale reduced basis functions can efficiently approximate the physical space of the wave function.

Expectations of physical quantities associated with different ε's. In this experiment, we solve (47) with the initial data $\psi_{\text{in}}(x) = (\frac{10}{\pi})^{1/4} e^{-20(x-0)^2}$ and the random potential (48), where the parameters in the random potential are the same as before. We choose different ε's in (47) to investigate the performance of our method. We define the expectation of position density as

$$\mathbb{E}(n^\varepsilon(t,\mathbf{x},\omega)) = \mathbb{E}\big(|\psi^\varepsilon(t,\mathbf{x},\omega)|^2\big), \tag{49}$$

and define the expectation of current density as

$$\mathbb{E}(J^\varepsilon(t,\mathbf{x},\omega)) = \mathbb{E}\big(\varepsilon \mathrm{Im}(\overline{\psi^\varepsilon(t,\mathbf{x},\omega)}\nabla\psi^\varepsilon(t,\mathbf{x},\omega))\big) = \mathbb{E}\left(\frac{1}{2i}(\overline{\psi^\varepsilon}\nabla\psi^\varepsilon - \psi^\varepsilon\nabla\overline{\psi^\varepsilon})\right). \tag{50}$$

In Figure 3, we plot expectations of densities associated with different ε's, i.e., $\varepsilon = \frac{1}{8}$, $\varepsilon = \frac{1}{16}$, $\varepsilon = \frac{1}{32}$, and $\varepsilon = \frac{1}{64}$. We observe the trend of convergence of these expectations with respect to ε. We want to emphasize that it is expensive to directly solve (47) with a very small ε and a random potential. However, our method is still efficient for computing this type of problem due to the model reduction in physical space.

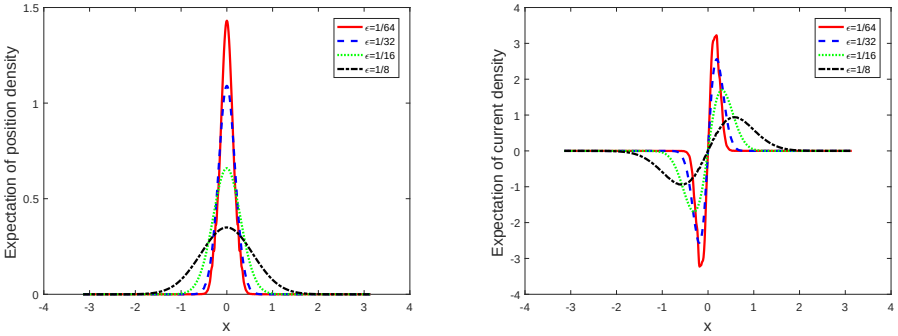

(a) expectation of position density. (b) expectation of current density.

FIG. 3. *Expectation of densities for different ε's at $T = 1$.*

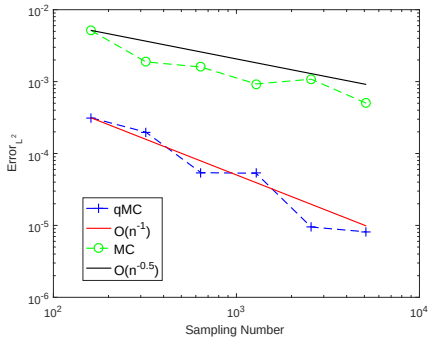

FIG. 4. *Comparison of the qMC method and the MC method. Convergence rate for qMC and MC are* 1.13 *and* 0.57*, respectively.*

5.2. Convergence in the random space. Again, we use the same example: (47)–(48) and $D = [-\pi, \pi]$, but we shall focus on the convergence of our method in a random space.

Convergence with respect to the number of qMC samples. In this numerical experiment, parameters of the random potential are the same as those in section 5.1, i.e., $\sigma = 1$ and $E = [\frac{1}{9}, \frac{1}{13}, \frac{1}{11}]$. Set $\varepsilon = \frac{1}{16}$ and the final time $T = 1$. For the reference solution, we choose the grid size to be $h = \frac{2\pi}{2048}$ and the number of qMC samples to be $n = 16000$. For our method, we choose the coarse grid size to be $H = \frac{2\pi}{256}$ and the number of multiscale reduced basis functions to be $m_k = 4$, such that the error in the physical space is small enough. To study the convergence rate of the qMC method, we change the number of the qMC samples successively from $n = 160$ to $n = 5120$ and compute the relative L^2 errors. We also compute the relative errors of the MC method with the same setting in the physical space and the same number of samples.

In Figure 4, we show the convergence result of our method. We find that the convergence rate of the qMC method is close to $O(n^{-1})$, which is consistent with results in Lemma 4.3 and in Theorem 4.5. Meanwhile, we compare the performance of the qMC method and the MC method. One can see that the convergence rate of the MC method is close to $O(n^{-\frac{1}{2}})$, which is also consistent with the error estimate

TABLE 2
Relative L^2 and H^1 errors in terms of sampling numbers of the qMC method in the offline stage.

qMC number	Error_{L^2}	Error_{H^1}
10	0.11800774	0.46614288
100	0.00136249	0.01497658
200	0.00130909	0.01455442
400	0.00129678	0.01449570

of the MC method. This result clearly shows that the qMC method is more accurate and efficient than the MC method.

Estimation of sampling numbers in the construction of multiscale reduced basis functions. In section 3.3, we obtained qualitative estimates on the choice of sampling numbers in the construction of multiscale reduced basis functions; see (25) and (26). In this experiment, we first generate Q qMC samples of the random potential $\{v^\varepsilon(x,\omega_q)\}_{q=1}^Q$. Then, for each sample $v^\varepsilon(x,\omega_q)$, we compute the corresponding multiscale basis functions. Finally, we construct multiscale reduced basis functions using the POD method. In the online stage, we solve (32) using the obtained multiscale reduced basis functions. The numerical setting for the reference solution is the same as before. For our method, we choose $H = \frac{2\pi}{128}$, $m_k = 3$, and $n = 2560$.

In Table 2, we show relative errors of numerical solutions obtained using different sampling numbers of the random potential. When the sampling number Q is small, say $Q = 10$, the error is big and the corresponding multiscale reduced basis functions cannot approximate the random space of the wave function well. When we increase Q, i.e., add more samples of the random potential in the construction of multiscale reduced basis functions, we obtain much better results. Notice that m_k is fixed to be 3. This means when Q is of order 100, the sampling number of the random potential is large enough to ensure the excellent approximation accuracy of multiscale reduced basis functions. One interesting topic on this issue is an optimal sampling strategy in the construction of multiscale reduced basis functions, which will be explored in a subsequent work.

Dependence of the number of qMC samples on ε and dimension of the random space m. We use the random potential $v^\varepsilon(x,\omega)$ with decaying terms satisfying Assumption 4.4:

$$v^\varepsilon(x,\omega) = 1 + \sum_{j=1}^{m} \frac{1}{j^2} \sin(jx)\xi_j(\omega) \tag{51}$$

in 1D physical domain $D = [-\pi,\pi]$ and $\xi_j(\omega)$'s are mean-zero and independent random variables uniformly distributed in $[-\sqrt{3},\sqrt{3}]$.

First, we set the random dimension to be $m = 8$, the final time $T = 1$. Three values of $\varepsilon = \frac{1}{4}, \frac{1}{8}$, and $\frac{1}{16}$ are tested. The reference solution is obtained in the same way as before. For the numerical solution we use the same fine mesh as that for the reference solution but for a different number of qMC samples. In Table 3, we list the number of qMC samples with respect to ε for the same accuracy requirement. It is observed that the number of qMC samples increases proportionally to $1/\varepsilon^{2.5}$.

Second, we fix $\varepsilon = \frac{1}{16}$ and change the dimension of the random space from $m = 1$, $m = 2$, $m = 4$, to $m = 8$. The reference solution and numerical solution are obtained in the same way as above. In Table 4, we list the number of qMC samples with respect to m for the same accuracy requirement. A linear growth of the number of qMC samples is observed when m is increased.

TABLE 3
Number of qMC samples for different ε's under the same accuracy requirement.

ε	qMC number	Error$_{L^2}$	Error$_{H^1}$
1/4	160	0.00469003	0.00654782
1/8	960	0.00399369	0.00767395
1/16	5120	0.00444144	0.00785192

TABLE 4
Number of qMC samples for different dimension m under the same accuracy requirement.

Dimension m	qMC number	Error$_{L^2}$	Error$_{H^1}$
1	520	0.00405535	0.00784524
2	1280	0.00341203	0.00667093
4	2560	0.00369911	0.00823515
8	5120	0.00444144	0.00785192

A slower decay of eigenvalues in the KL expansion of the random potential requires more qMC samples. For instance, when $v^\varepsilon(x,\omega) = 1 + \sum_{j=1}^m \frac{1}{j}\sin(jx)\xi_j(\omega)$, we observed a quadratic growth of the number of qMC samples when m is increased. However, the qMC method is still very efficient in solving this difficult problem. Moreover, the qMC method can be implemented in a parallel fashion to further improve its efficiency.

5.3. Investigation of Anderson localization. In this section, we investigate the Anderson localization phenomenon for the semiclassical Schrödinger equation using our method. Physically, when the Anderson localization happens, the electron transport stops under the strong disorder and the short-range correlation in space. We emphasize that the short-range correlation is important for localization, while the long-range correlation may lead to delocalization [16, 39]. To numerically measure the localization of a wave function, we define

$$A(t) = \mathbb{E}\left[\int_D |\mathbf{x}|^2 |\psi^\varepsilon(t,\mathbf{x},\omega)|^2 \mathrm{d}\mathbf{x}\right], \tag{52}$$

where $\mathbf{x} = x$ when $d = 1$ and $\mathbf{x} = (x_1, x_2)$ when $d = 2$.

1D Schrödinger equation. Consider the Schrödinger equation (47) with the periodic boundary condition over $D = [-\pi, \pi]$. To approximate the spatially white noise in the potential, we employ the m-term KL expansion

$$v^\varepsilon(x,\omega) = \sigma \sum_{j=1}^m \sin(jx)\frac{1}{j^\beta}\xi_j(\omega), \tag{53}$$

where $\xi_j(\omega)$'s are mean-zero and i.i.d. random variables uniformly distributed in $[-\sqrt{3}, \sqrt{3}]$. When $\beta = 0$, $v^\varepsilon(x,\omega)$ converges to the spatially white noise as $m \to \infty$. σ controls the strength of randomness.

The setup is as follows: the fine-scale grid size $h = \frac{2\pi}{600}$, the coarse grid size $H = \frac{2\pi}{100}$, $\varepsilon = \frac{1}{8}$, $\sigma = 5$, and the initial datum $\psi_{\text{in}}(x)$ is

$$\psi_{\text{in}}(x) = \left(\frac{10}{\pi}\right)^{1/4} e^{-20(x-0)^2}. \tag{54}$$

In Figure 5(a), we plot $A(t)$ as a function of t for different m's when $\beta = 0$. When m increases, the wave function quickly enters a localization phase. In Figure 5(b), we

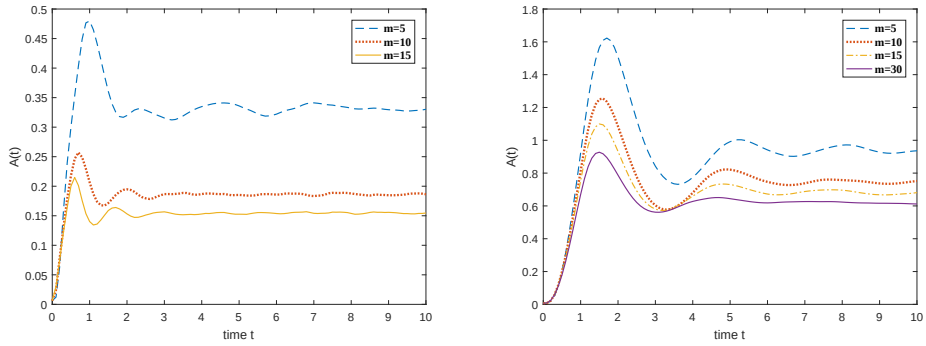

(a) $\beta = 0$. (b) $\beta = 1$.

FIG. 5. *Anderson localization for different parameters.*

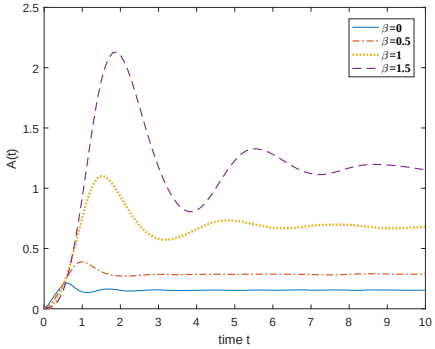

FIG. 6. *Anderson localization for different β's.*

plot the time evolution of $A(t)$ for different m's when $\beta = 1$. Notice that $\beta = 1$ leads to a slower decay in the KL expansion of the random potential (53). Therefore, more terms need to be added to the KL expansion in order to generate a localization phase for the wave function. We also plot the time evolution of $A(t)$ for β ranging from 0 to 1.5 when $\sigma = 5$, $m = 15$ in Figure 6. The localization phase is much easier to be approached as β goes to 0. Besides, we also observe that a larger σ makes the wave function approach the localization phase more quickly with other parameters fixed. To sum up, the localization phase can be approached more easily when we have more terms in the KL expansion, a shorter range of randomness, or stronger randomness.

Before we end the study of the Anderson localization in 1 dimension, we compare the performance of the qMC-based method and the sparse grid collocation (SGC)-based method. The setup is the same as before.

When $m = 2$, we choose the accuracy level $l = 18$ and $l = 20$ in the SGC method, which gives us $Q = 449$ and $Q = 705$ sparse grid points, respectively. In the qMC method, we choose sample numbers $Q = 1000$ and $Q = 2000$. In Figure 7, we plot the time evolution of $A(t)$ obtained by different methods with different points or samples. We find that when the random dimension is low, the performance of the SGC method is as good as the qMC method.

To study the Anderson localization, we need to choose m large enough in the random potential (53). When $m = 15$, we choose the accuracy level $l = 4$ and $l = 5$

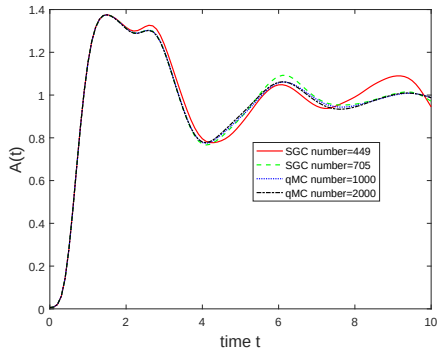

FIG. 7. *Time evolution of $A(t)$ obtained from different methods.*

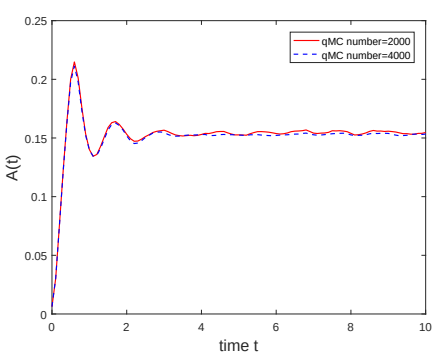

(a) $m = 15$ in the qMC method.

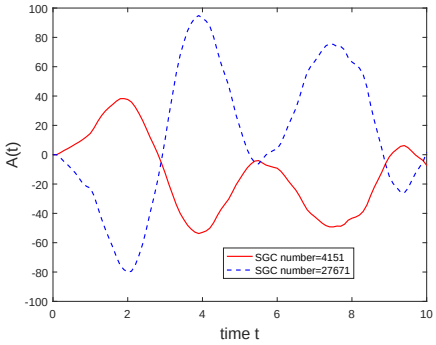

(b) $m = 15$ in the qMC sparse grid collocation method.

FIG. 8. *Time evolution of $A(t)$ for different methods.*

in the SGC method, which gives us $Q = 4151$ and $Q = 27671$ sparse grid points, respectively. In the qMC method, we choose sample number $Q = 2000$ and $Q = 4000$.

In Figure 8(a), we see the convergence behavior of the qMC method and observe the localization phenomenon. In Figure 8(b), however, we do not see the convergence behavior of the SGC method even when the number of sparse grid points is much larger than the qMC sample points. The negative value of $A(t)$ in Figure 8(b) is wrong; it is caused by the negative quadrature weights in the SGC method.

In terms of computational cost, the qMC method with $Q = 4000$ samples costs about 10600 seconds, while the SGC method with $Q = 27671$ grid points costs 73328 seconds. One may choose higher accuracy levels in the SGC that further increases the computational cost. This numerical result suggests that the qMC-based method is superior to the SGC-based method in simulating the Anderson localization phenomenon when the random dimension is large. More in-depth studies on the qMC method and SGC method will be our future research plan.

2D Schrödinger equation. Consider the Schrödinger equation (32) over $D = [-\pi, \pi] \times [-\pi, \pi]$ and

$$v^{\varepsilon}(x_1, x_2, \omega) = \sigma \sum_{j=1}^{m} \sin(jx_1) \sin(jx_2) \frac{1}{j^{\beta}} \xi_j(\omega), \tag{55}$$

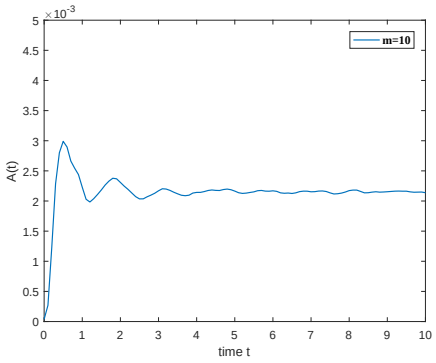

FIG. 9. *Anderson localization when* $\sigma = 5$ *and* $\beta = 0$ *in* 2 *dimensions.*

where the setting of $\xi_j(\omega)$'s is the same as the 1D case; σ, m, and β are parameters that control the random potential. We choose $\sigma = 5$, $\beta = 0$, and $\varepsilon = \frac{1}{4}$ here. Notice that $\beta = 0$ and (55) is used to model a short-range random potential.

For our method, the fine grid size is $h = \frac{2\pi}{400}$ and the coarse grid size is $H = \frac{2\pi}{100}$. In Figure 9, we plot the time evolution of $A(t)$ when $m = 10$. One can see that the wave function approaches a localization phase when $t = 4$. If we approximate the random space of the wave function by the PCE method, the computation cost grows quickly since we need a significant amount of polynomial basis functions. Other strategies, such as the stochastic collocation method and the sparse grid method, suffer from a similar issue. However, due to its nonintrusive nature, the proposed qMC-based method is efficient to solve this problem in the presence of a (relatively) large random space.

6. Conclusions and discussions. In this paper, we have proposed a multiscale reduced basis method to solve the Schrödinger equation with random potential in the semiclassical regime. The physical space of the solution is approximated by a set of localized multiscale basis functions based on an optimization approach. The POD method is then applied to extract a smaller number of multiscale reduced basis functions to further reduce the computational cost without loss of approximation accuracy. The number of samples to learn the multiscale reduced basis functions is also analyzed, which provides guidance in practical computations. The qMC method is employed to approximate the random space of the solution. Approximation accuracy of the proposed method is analyzed. It is observed that the spatial grid size is proportional to the semiclassical parameter and the number of samples is inversely proportional to a power of the same parameter. Finally we present several numerical examples to demonstrate the accuracy and efficiency of the proposed method. Moreover, we investigate the Anderson localization phenomenon for the Schrödinger equation with correlated random potentials in both 1 dimension and 2 dimensions.

There are two lines of work which deserve explorations in the near future. First, in the physics community, the random Schrödinger equation in higher dimensions (2 dimensions and 3 dimensions) has been frequently used to study Anderson localization; see [19] for example. Though the random potential is assumed to be white noise without spatial correlation in the original paper [2], the correlated random potential is also found to generate localized states; see [12] for example. In the mathematics community, it is also known that the existence or nonexistence of Anderson localiza-

tion for some types of 3D Schrödinger equations with random potentials remains open [16]. It is thus quite interesting to explore this issue from a numerical perspective. Second, we plan to solve the Helmholtz equation in random media using the multiscale reduced basis method developed in this paper.

REFERENCES

[1] M. Aizenman and S. Molchanov, *Localization at large disorder and at extreme energies: An elementary derivation*, Comm. Math. Phys. (2), 157 (1993), pp. 245–278.

[2] P. W. Anderson, *Absence of diffusion in certain random lattices*, Phys. Rev. (2), 109 (1958), pp. 1492–1505.

[3] D. Arnold, G. David, D. Jerison, S. Mayboroda, and M. Filoche, *Effective confining potential of quantum states in disordered media*, Phys. Rev. Lett., 116 (2016), 056602.

[4] I. Babuska and R. Lipton, *Optimal local approximation spaces for generalized finite element methods with application to multiscale problems*, Multiscale Model. Simul., 9 (2011), pp. 373–406.

[5] W. Bao, S. Jin, and P. A. Markowich, *On time-splitting spectral approximations for the Schrödinger equation in the semiclassical regime*, J. Comput. Phys., 175 (2002), pp. 487–524.

[6] G. Berkooz, P. Holmes, and J. L. Lumley, *The proper orthogonal decomposition in the analysis of turbulent flows*, Annu. Rev. Fluid Mech., 25 (1993), pp. 539–575.

[7] H.-J. Bungartz and M. Griebel, *Sparse grids*, Acta Numer., 13 (2004), pp. 147–269.

[8] J. Chen, S. Li, and Z. Zhang, *Efficient multiscale methods for the semiclassical Schrödinger equation with time-dependent potentials*, Comput. Methods. Appl. Mech. Engrg., 369 (2020), 113232.

[9] J. Chen, D. Ma, and Z. Zhang, *Convergence of a Multiscale Finite Element Method for the Schrödinger Equation with Multiscale Potentials*, manuscript.

[10] J. Chen, D. Ma, and Z. Zhang, *A multiscale finite element method for the Schrödinger equation with multiscale potentials*, SIAM J. Sci. Comput., 41 (2019), pp. B1115–B1136.

[11] R. Delgadillo, J. Lu, and X. Yang, *Gauge-invariant frozen Gaussian approximation method for the Schrodinger equation with periodic potentials*, SIAM J. Sci. Comput., 38 (2016), pp. A2440–A2463.

[12] T. Devakul and D. A. Huse, *Anderson localization transitions with and without random potentials*, Phys. Rev. B(3), 96 (2017), 214201.

[13] J. Dick, F. Y. Kuo, and I. H. Sloan, *High-dimensional integration: The quasi-Monte Carlo way*, Acta Numer., 22 (2013), pp. 133–288.

[14] C. R. Dietrich and G. N. Newsam, *Fast and exact simulation of stationary Gaussian processes through circulant embedding of the covariance matrix*, SIAM J. Sci. Comput., 18 (1997), pp. 1088–1107.

[15] Y. Efendiev and T. Y. Hou, *Multiscale Finite Element Methods: Theory and Applications*, Surv. Tutor. Appl. Math. Sci. 4, Springer, New York, 2009.

[16] L. Erdos, *Lecture Notes on Quantum Brownian Motion*, preprint, https://arxiv.org/abs/1009.0843, (2010).

[17] E. Faou, V. Gradinaru, and C. Lubich, *Computing semiclassical quantum dynamics with Hagedorn wavepackets*, SIAM J. Sci. Comput., 31 (2009), pp. 3027–3041.

[18] E. Faou and C. Lubich, *A Poisson integrator for Gaussian wavepacket dynamics*, Comput. Vis. Sci., 9 (2006), pp. 45–55.

[19] M. Filoche and S. Mayboroda, *Universal mechanism for Anderson and weak localization*, Proc. Natl. Acad. Sci. USA, 109 (2012), pp. 14761–14766.

[20] J. Fröhlich and T. Spencer, *Absence of diffusion in the Anderson tight binding model for large disorder or low energy*, Comm. Math. Phys., 88 (1983), pp. 151–184.

[21] R. G. Ghanem and P. D. Spanos, *Stochastic Finite Elements: A Spectral Approach*, Dover, Minneola, NY, 2003.

[22] I. G. Graham, F. Y. Kuo, J. A. Nichols, R. Scheichl, C. Schwab, and I. H. Sloan, *Quasi-Monte Carlo finite element methods for elliptic PDEs with lognormal random coefficients*, Numer. Math., 131 (2015), pp. 329–368.

[23] T. Hou, X. Wu, and Z. Cai, *Convergence of a multiscale finite element method for elliptic problems with rapidly oscillating coefficients*, Math. Comp., 68 (1999), pp. 913–943.

[24] T. Y. Hou, D. Ma, and Z. Zhang, *A model reduction method for multiscale elliptic Pdes with random coefficients using an optimization approach*, Multiscale Model. Simul., 17 (2019), pp. 826–853.

[25] T. Y. Hou and X. Wu, *A multiscale finite element method for elliptic problems in composite materials and porous media*, J. Comput. Phys., 134 (1997), pp. 169–189.
[26] T. Y. Hou and P. Zhang, *Sparse operator compression of higher-order elliptic operators with rough coefficients*, Res. Math. Sci., 4 (2017), 24.
[27] S. Jin, L. Liu, G. Russo, and Z. Zhou, *Gaussian Wave Packet Transform Based Numerical Scheme for the Semi-Classical Schrödinger Equation with Random Inputs*, https://arxiv.org/abs/1903.08740 (2019).
[28] S. Jin, P. Markowich, and C. Sparber, *Mathematical and computational methods for semiclassical Schrödinger equations*, Acta Numer., 20 (2011), pp. 121–209.
[29] S. Jin, P. Qi, and Z. Zhang, *An Eulerian surface hopping method for the Schrödinger equation with conical crossings*, Multiscale Model. Simul., 9 (2011), pp. 258–281.
[30] S. Jin, H. Wu, X. Yang, et al., *Gaussian beam methods for the Schrödinger equation in the semi-classical regime: Lagrangian and Eulerian formulations*, Commun. Math. Sci., 6 (2008), pp. 995–1020.
[31] K. Karhunen, *Uber lineare methoden in der Wahrscheinlichkeitsrechnung*, Ann. Acad. Sci. Fenn., 37 (1947), pp. 1–79.
[32] V. I. Karpman, *Stabilization of soliton instabilities by higher-order dispersion: Fourth-order nonlinear Schrödinger-type equations*, Phys. Rev. E(3), 53 (1996), pp. R1336–R1339.
[33] S. Li and Z. Zhang, *Computing eigenvalues and eigenfunctions of Schrödinger equations using a model reduction approach*, Commun. Comput. Phys., 24 (2018), pp. 1073–1100.
[34] M. Loève, *Probability theory*, Vol. II, 4th ed., Grad. Texts in Math. 46, Springer, New York, 1978.
[35] A. Målqvist and D. Peterseim, *Localization of elliptic multiscale problems*, Math. Comp., 83 (2014), pp. 2583–2603.
[36] B. Min, T. Li, M. Rosenkranz, and W. Bao, *Subdiffusive spreading of a Bose-Einstein condensate in random potentials*, Phys. Rev. A(3), 86 (2012), 053612.
[37] N. Mott, *Metal-insulator transitions*, CRC Press, Boca Raton, FL, 1990.
[38] F. Nobile, R. Tempone, and C. G. Webster, *A sparse grid stochastic collocation method for partial differential equations with random input data*, SIAM J. Numer. Anal., 46 (2008), pp. 2309–2345.
[39] P. Nosov, I. Khaymovich, and V. Kravtsov, *Correlation-induced localization*, Phys. Rev. B(3), 99 (2019), 104203.
[40] H. Owhadi, *Bayesian numerical homogenization*, Multiscale Model. Simul., 13 (2015), pp. 812–828.
[41] H. Owhadi, *Multigrid with rough coefficients and multiresolution operator decomposition from hierarchical information games*, SIAM Rev., 59 (2017), pp. 99–149.
[42] C. Schwab and R. A. Todor, *Karhunen–Loève approximation of random fields by generalized fast multipole methods*, J. Comput. Phys., 217 (2006), pp. 100–122.
[43] L. Sirovich, *Turbulence and the dynamics of coherent structures.* I. *Coherent structures*, Quart. Appl. Math., 45 (1987), pp. 561–571.
[44] N. M. Tanushev, J. Qian, and J. V. Ralston, *Mountain waves and Gaussian beams*, Multiscale Model. Simul., 6 (2007), pp. 688–709.
[45] Z. Wu and Z. Huang, *A Bloch decomposition-based stochastic Galerkin method for quantum dynamics with a random external potential*, J. Comput. Phys., 317 (2016), pp. 257–275.
[46] D. Xiu and G. E. Karniadakis, *Modeling uncertainty in flow simulations via generalized polynomial chaos*, J. Comput. Phys., 187 (2003), pp. 137–167.